

Neutron electric dipole moment from lattice QCD

E. Shintani,¹ S. Aoki,^{1,2} N. Ishizuka,^{1,3} K. Kanaya,¹ Y. Kikukawa,⁴
Y. Kuramashi,^{1,3} M. Okawa,⁵ Y. Taniguchi,^{1,3} A. Ukawa,^{1,3} and T. Yoshié^{1,3}

(CP-PACS Collaboration)

¹ *Graduate School of Pure and Applied Sciences,*

University of Tsukuba, Tsukuba, Ibaraki 305-8571, Japan

² *Riken BNL Research Center, Brookhaven National Laboratory, Upton, 11973, USA*

³ *Center for Computational Sciences,*

University of Tsukuba, Tsukuba, Ibaraki 305-8577, Japan

⁴ *Department of Physics, Nagoya University, Nagoya 464-8602, Japan*

⁵ *Department of Physics, Hiroshima University,*

Higashi-Hiroshima, Hiroshima 739-8526, Japan

(Dated: May 24, 2019)

Abstract

We carry out a feasibility study for the lattice QCD calculation of the neutron electric dipole moment (NEDM) in the presence of the θ term. We develop the strategy to obtain the nucleon EDM from the CP-odd electromagnetic form factor F_3 at small θ , in which NEDM is given by $\lim_{q^2 \rightarrow 0} \theta F_3(q^2)/(2m_N)$ where q is the momentum transfer and m_N is the nucleon mass. We first derive a formula which relates F_3 , a matrix element of the electromagnetic current between nucleon states, with vacuum expectation values of nucleons and/or the current. In the expansion of θ , the parity-odd part of the nucleon-current-nucleon three-point function contains contributions not only from the parity-odd form factors but also from the parity-even form factors multiplied by the parity-odd part of the nucleon two-point function, and therefore the latter contribution must be subtracted to extract F_3 . We then perform an explicit lattice calculation employing the domain-wall quark action with the RG improved gauge action in quenched QCD at $a^{-1} \simeq 2$ GeV on a $16^3 \times 32 \times 16$ lattice. At the quark mass $m_f a = 0.03$, corresponding to $m_\pi/m_\rho \simeq 0.63$, we accumulate 730 configurations, which allow us to extract the parity-odd part in both two- and three-point functions. Employing two different Dirac γ matrix projections, we show that a consistent value for F_3 cannot be obtained without the subtraction described above. We obtain $F_3(q^2 \simeq 0.58 \text{ GeV}^2)/(2m_N) = -0.024(5) \text{ e}\cdot\text{fm}$ for the neutron and $F_3(q^2 \simeq 0.58 \text{ GeV}^2)/(2m_N) = 0.021(6) \text{ e}\cdot\text{fm}$ for the proton.

PACS numbers: 11.15.Ha, 11.30.Rd, 12.39.Fe, 12.38.Gc

I. INTRODUCTION

In the strong interaction, one of the most stringent constraints on possible violation of parity (P) and time-reversal (T) symmetry comes from the measurement of the electric dipole moment (EDM) for neutron (NEDM) and proton (PEDM) $\vec{d}_{n,p}$. The current upper bound is given by

$$|\vec{d}_n| < 6.3 \times 10^{-26} \text{ e} \cdot \text{cm} \text{ (90\% C.L.)} \quad (1)$$

for neutron[1], and

$$|\vec{d}_p| < 5.4 \times 10^{-24} \text{ e} \cdot \text{cm} \quad (2)$$

for proton[2], which are estimated from the results for EDM of mercury atom ^{199}Hg given by $(d(^{199}\text{Hg})) < 2.1 \times 10^{-28} \text{ e} \cdot \text{cm} \text{ (95\% C.L.)}$ [3])

On the other hand, QCD, which is regarded as the fundamental theory of the strong interaction, allows a gauge invariant, renormalizable CP odd operator in the Lagrangian, called the θ term:

$$i \frac{\theta}{32\pi^2} \int d^4x \tilde{G}_{\mu\nu}(x) G_{\mu\nu}(x), \quad \tilde{G}_{\mu\nu}(x) = \frac{1}{4} \varepsilon_{\mu\nu\alpha\beta} G_{\alpha\beta}(x) \quad (3)$$

in Euclidean space-time with $G_{\mu\nu}$ the field strength of gluon. Some model estimations[4, 5] yield

$$|\vec{d}_n| \sim \theta \times O(10^{-15} \sim 10^{-16}) \text{ e} \cdot \text{cm}, \quad (4)$$

and this leads to a bound $\theta \lesssim O(10^{-10})$. Hence θ must be small or even must vanish in QCD.

A smallness of θ in the QCD sector, however, is not protected in the presence of the electroweak sector of the standard model, where the quark mass matrix, arising from Yukawa couplings to the Higgs field, may be written as

$$\bar{\psi}_i^R(x) M_{ij} \psi_j^L(x) + \bar{\psi}_i^R(x) M_{ij}^\dagger \psi_j^L(x), \quad (5)$$

where ψ_L and ψ_R represent left and right handed quark fields with flavor indices i, j . Diagonalizing the mass matrix and making it real, the parameter θ becomes

$$\theta = \theta_{\text{QCD}} + \arg \det M, \quad (6)$$

where θ_{QCD} is the original θ parameter in QCD. Therefore, either θ_{QCD} and $\arg \det M$ are individually small, or the two contributions cancel out to the degree that the experimental

upper bound on NEDM is satisfied. In either of the two cases, it seems necessary to explain why Nature chooses such a small value for θ ; this is the “strong CP problem”. One of the most attractive explanations proposed so far is the Peccei-Quinn mechanism[6]. Unfortunately, the axion, a new particle predicted by this mechanism, has not been experimentally observed yet.

The present model estimations of the hadronic contribution to NEDM, $|\vec{d}_n|/\theta$, are maybe enough to convince us of the smallness of θ [7, 8]. However, a theoretically reliable and accurate estimation for NEDM will be required to determine the value of θ , if non-zero value of NEDM is observed in future experiments. Lattice QCD calculations seem ideal for this requirement. Indeed more than 15 years ago the first attempt was made to estimate NEDM in a quenched lattice QCD simulation[9] by calculating the spin dependent energy difference of the nucleon in the presence of the uniform static electric field. In this simulation, the θ was converted to the phase of the quark mass term by the chiral rotation, and a non-zero value of NEDM was obtained for non-zero θ . Unfortunately this non-zero value of NEDM turned out[10] to be a lattice artifact due to the explicit chiral symmetry breaking of the Wilson fermion action employed in the simulation; if the θ term appears in the quark mass, an additional disconnected contribution must be included in the quenched calculation of Ref.[9].

After this attempt, there has been no further lattice investigation on this problem for a long time. Recently, a new lattice strategy [11] for the extraction of NEDM has been proposed, and a lattice related investigation on NEDM has been made[12]. Also, a preliminary lattice QCD result of NEDM estimated from the nucleon electromagnetic three-point function has been reported at the lattice 2004 conference[13]. The value of NEDM divided by θ is consistent with zero within statistical errors in this calculation, however. In all attempts, an expansion in θ have been used to avoid the complex action due to the θ term.

Since chiral symmetry seems important in the calculation of NEDM[14], it may be preferable to use lattice fermion formulations having good chiral symmetry, such as the domain-wall fermion[15] or the overlap fermion[16]. In these formulations, the bosonic definitions of the topological charge agree well with the fermionic definitions. In fact the domain-wall fermion was employed in Ref.[13].

In this paper we propose a new method to calculate NEDM in lattice QCD. We consider the strategy of extracting NEDM from the CP-odd part of the electromagnetic form

factor of the nucleon, as in the recent lattice calculation [13] as well as in some past model calculations [7, 8]. We first examine the θ dependence of the three-point (two nucleons and the electromagnetic current) function by expanding up to first order in θ under the assumption that θ has fairly small value. An important finding is that the parity-odd part of the three-point function contains a contribution coming from the parity-even form factors multiplied by the parity-odd part of the nucleon two-point function. This contribution has to be subtracted from the three-point function in order to properly extract the CP-odd form factor relevant for NEDM. This point is not considered in Ref.[13]. We present the formula to extract the relevant form factor in terms of the nucleon two- and three-point functions, which is valid not only for lattice simulations but also for general cases as long as chiral symmetry of quarks is well formulated in the calculations.

We test our formula in a lattice QCD simulation using the domain-wall fermion in the quenched approximation. A renormalization group (RG) improved gauge action is employed based on our experience that the residual chiral symmetry breaking due to a finite fifth dimensional extent is smaller than in the case for the plaquette gauge action at a similar lattice spacing[17]. Since our primary purpose is to check the feasibility of the lattice QCD calculation of NEDM based on our formula, we focus on accumulating the statistics to obtain a sufficient sampling of topological charge on a $16^3 \times 32 \times 16$ lattice at $a^{-1} \simeq 2$ GeV with the quark mass of $m_f = 0.03$, corresponding to $m_\pi/m_\rho \simeq 0.63$. Our numerical results reveal that the contribution to the three-point function from the parity-even form factors multiplied by the parity-odd part of the nucleon two-point function is really significant. We demonstrate the correctness of our formula by showing that two independent ways to extract the relevant form factor give consistent results only if the contribution from the parity-even form factors is properly subtracted.

This paper is organized as follows. In Sec. II we derive the formula to extract the relevant form factor in terms of the two- and three-point functions to first order in the expansion in θ . Section III contains simulation parameters and technical details. In Sec. IV we present the simulation results for the CP-odd form factors together with the CP-even ones. It is demonstrated that we cannot obtain the correct value for the CP-odd form factor without subtracting the contribution from the parity-even form factors. We conclude our investigation in Sec. V.

II. NUCLEON ELECTRIC DIPOLE MOMENT FROM CORRELATION FUNCTIONS

A. Form factors and EDM

We consider the electromagnetic form factors of the nucleon, defined by

$$\langle N(\vec{p}, s) | J_\mu^{\text{EM}} | N(\vec{p}', s') \rangle = \bar{u}(\vec{p}, s) \left[\frac{F_3(q^2)}{2m_N} q_\nu \sigma_{\mu\nu} \gamma_5 + \cdots \right] u(\vec{p}', s'), \quad (7)$$

where $q = p - p'$ is the momentum transfer, $|N(\vec{p}, s)\rangle$ is the on-shell nucleon state with momentum \vec{p} , energy $p_0 = \sqrt{m_N^2 + \vec{p}^2}$ and helicity s . The electromagnetic current for quarks, J_μ^{EM} , is given by

$$J_\mu^{\text{EM}} = \sum_f e_f \bar{\psi}_f \gamma_\mu \psi_f, \quad (8)$$

where ψ_f is the quark field with flavor f and the electric charge e_f .

In the small momentum transfer limit, $q \rightarrow 0$, the above form factor is described by the following effective interaction:

$$\bar{N}(x) \left[\frac{F_3(0)}{2m_N} \sigma_{\mu\nu} \gamma_5 \partial_\nu A_\mu(x) + \cdots \right] N(x), \quad (9)$$

where $A_\mu(x)$ is the U(1) electromagnetic field. We can define the electric dipole moment \vec{d}_N as

$$|\vec{d}_N| = \lim_{q^2 \rightarrow 0} \frac{F_3(q^2)}{2m_N} = \frac{F_3(0)}{2m_N}. \quad (10)$$

So far we do not specify CP properties of the system and therefore θ dependences are omitted in the above expressions.

B. Extraction of form factors from correlation functions

In the lattice calculation we must extract the form factors from the three-point correlation functions such as

$$G_{NJ_\mu N}^\theta(q, t, \tau) \equiv \langle \theta | N(\vec{p}, t) J_\mu^{\text{EM}}(\vec{q}, \tau) \bar{N}(\vec{p}', 0) | \theta \rangle, \quad (11)$$

where $N(\vec{p}, t)$ and $\bar{N}(\vec{p}, t)$ are the interpolating fields of the nucleon at time t , which contain annihilation and creation operators with momentum \vec{p} . Here $|\theta\rangle$ is the θ vacuum, which may be defined as

$$|\theta\rangle = e^{i\theta Q_5} |0\rangle, \quad Q_5 = \int d^3x K_0(\vec{x}, t), \quad (12)$$

using the conserved (but gauge non-invariant) chiral current K_μ . Throughout this paper, we do not use the explicit representation of $|\theta\rangle$. Inserting the complete set of states between the interpolating fields and the current, we obtain

$$G_{NJ_\mu N}^\theta(q, t, \tau) = e^{-E_{N^\theta}(t-\tau)} e^{-E'_{N^\theta}t} \times \sum_{s, s'} \langle \theta | N | N^\theta(\vec{p}, s) \rangle \langle N^\theta(\vec{p}, s) | J_\mu^{\text{EM}} | N^\theta(\vec{p}', s') \rangle \langle N^\theta(\vec{p}', s') | \bar{N} | \theta \rangle + \dots, \quad (13)$$

where $E_{N^\theta} = \sqrt{\vec{p}^2 + m_{N^\theta}^2}$, $E'_{N^\theta} = \sqrt{\vec{p}'^2 + m_{N^\theta}^2}$, and the dots represent exponentially suppressed contributions, which are assumed to be negligible. Hereafter we represent explicitly superscript of θ on θ vacuum effects. Since the interpolating fields N and \bar{N} can be expanded as

$$\begin{aligned} N(\vec{p}, 0) &= Z_N^\theta \sum_s a_{N^\theta}(\vec{p}, s) u_N^\theta(\vec{p}, s) + \dots, \\ \bar{N}(\vec{p}, 0) &= (Z_N^\theta)^* \sum_s a_{N^\theta}^\dagger(\vec{p}, s) \bar{u}_N^\theta(\vec{p}, s) + \dots, \end{aligned} \quad (14)$$

we have

$$\begin{aligned} \langle \theta | N | N^\theta(\vec{p}, s) \rangle &= Z_N^\theta u_N^\theta(\vec{p}, s), \\ \langle N^\theta(\vec{p}', s') | \bar{N} | \theta \rangle &= (Z_N^\theta)^* \bar{u}_N^\theta(\vec{p}', s'), \end{aligned} \quad (15)$$

since

$$|N^\theta(\vec{p}, s)\rangle = a_{N^\theta}^\dagger(\vec{p}, s) |\theta\rangle \quad (16)$$

$$\langle N^\theta(\vec{p}, s) | = \langle \theta | a_{N^\theta}(\vec{p}, s). \quad (17)$$

In eq. (14) the dots represent contributions from all other possible states including the negative energy state of the nucleon, the negative parity states or other excited states. Except a special case considered in the appendix, we will not consider these states in this paper. The spinors $u_N^\theta(\vec{p}, s)$ and $\bar{u}_N^\theta(\vec{p}, s)$ are on-shell nucleon wave functions which satisfy the Dirac equation:

$$(i\gamma \cdot p + m_{N^\theta} e^{-if_N(\theta)\gamma_5}) u_N^\theta(\vec{p}, s) = \bar{u}_N^\theta(\vec{p}, s) (i\gamma \cdot p + m_{N^\theta} e^{-if_N(\theta)\gamma_5}) = 0. \quad (18)$$

Since CP is broken in the θ vacuum, a CP non-invariant phase factor $e^{if_N(\theta)\gamma_5}$ can appear in the mass term. This means that $f_N(\theta)$ must be odd in θ , while m_N and Z_N are even in θ .

Therefore we have

$$\begin{aligned} m_{N^\theta} &= m_N + O(\theta^2), \quad Z_N^\theta = Z_N + O(\theta^2) \\ f_N(\theta) &= f_N^1 \theta + O(\theta^3) \end{aligned} \quad (19)$$

for small θ . The bi-spinor projection satisfies

$$\sum_s u_N^\theta(\vec{p}, s) \bar{u}_N^\theta(\vec{p}, s) = \frac{-i\gamma \cdot p + m_{N^\theta} e^{if_N(\theta)\gamma_5}}{2E_{N^\theta}} \quad (20)$$

with the normalization that $\bar{u}_N^\theta(\vec{p}, s) u_N^\theta(\vec{p}, s') = \frac{m_{N^\theta} \cos f_N(\theta)}{E_{N^\theta}} \delta_{s,s'}$.

The form factor, which we wish to extract from the three-point function, is written as

$$\langle N^\theta(\vec{p}, s) | J_\mu^{\text{EM}} | N^\theta(\vec{p}', s') \rangle = \bar{u}_N^\theta(\vec{p}, s) W_\mu^\theta(q) u_N^\theta(\vec{p}', s') \quad (21)$$

It satisfies

$$\bar{u}_N^\theta(\vec{p}, s) q_\mu W_\mu^\theta(q) u_N^\theta(\vec{p}', s') = 0 \quad (22)$$

from the current conservation $\partial_\mu J_\mu^{\text{EM}} = 0$. Taking account of the parity properties, the form factors in general should have the form that

$$W_\mu^\theta(q) = g(\theta^2) W_\mu^{\text{even}}(q) + i\theta h(\theta^2) W_\mu^{\text{odd}}(q), \quad (23)$$

where we take $g(0) = h(0) = 1$ for their normalizations and

$$W_\mu^{\text{even}}(q) = \gamma_\mu F_1(q^2) + \frac{F_2(q^2)}{2m_N} q_\nu \sigma_{\mu\nu}, \quad (24)$$

$$W_\mu^{\text{odd}}(q) = \frac{F_3(q^2)}{2m_N} q_\nu \sigma_{\mu\nu} \gamma_5 + F_A(q^2) (q_\mu \gamma \cdot q - \gamma_\mu q^2) \gamma_5 \quad (25)$$

with $\sigma_{\mu\nu} = i[\gamma_\mu, \gamma_\nu]/2$. Here $F_{1,2}(q^2)$ are the electromagnetic form factors and $F_A(q^2)$ is called ‘‘anapole form factor’’. As mentioned in Sec. II A, $F_3(0)/(2m_N)$ gives the nucleon electric dipole moment. For small θ , we can expand $g(\theta^2) = 1 + O(\theta^2)$ and $h(\theta^2) = 1 + O(\theta^2)$.

Using all the necessary expressions and expanding in terms of θ , we obtain

$$\begin{aligned} G_{NJ_\mu N}^\theta(q, t, \tau) &= |Z_N|^2 e^{-E_N(t-\tau)} e^{-E'_N t} \frac{-i\gamma \cdot p + m_N(1 + if_N^1 \theta \gamma_5)}{2E_N} \\ &\times [W_\mu^{\text{even}}(q) + i\theta W_\mu^{\text{odd}}(q)] \frac{-i\gamma \cdot p' + m_N(1 + if_N^1 \theta \gamma_5)}{2E'_N} + O(\theta^2). \end{aligned} \quad (26)$$

On the other hand, $G_{NJ_\mu N}^\theta(q, t, \tau)$ can be evaluated by the path integral as

$$\begin{aligned} G_{NJ_\mu N}^\theta(q, t, \tau) &= \langle \vec{N}(\vec{p}, t) J_\mu^{\text{EM}}(\vec{q}, \tau) \bar{N}(\vec{p}', 0) e^{i\theta Q} \rangle \\ &= G_{NJ_\mu N}(q, t, \tau) + i\theta G_{NJ_\mu N}^Q(q, t, \tau) + O(\theta^2) \end{aligned} \quad (27)$$

with

$$G_{NJ_\mu N}(q, t, \tau) = \langle \vec{N}(\vec{p}, t) J_\mu^{\text{EM}}(\vec{q}, \tau) \bar{N}(\vec{p}', 0) \rangle, \quad (28)$$

$$G_{NJ_\mu N}^Q(q, t, \tau) = \langle \vec{N}(\vec{p}, t) J_\mu^{\text{EM}}(\vec{q}, \tau) \bar{N}(\vec{p}', 0) Q \rangle, \quad (29)$$

where N , \bar{N} , and J_μ^{EM} are c-number operators in the path-integral, albeit using the same notation as the quantum operators, and Q is the topological charge, defined by

$$Q = \frac{1}{32\pi^2} \int d^4x \tilde{G}_{\mu\nu}(x) G_{\mu\nu}(x) \quad (30)$$

in the continuum theory. The symbol $\langle \mathcal{O} \rangle$ denotes the path-integral average of an operator \mathcal{O} in QCD with $\theta = 0$, which is given by

$$\langle \mathcal{O} \rangle = \int \mathcal{D}\psi \mathcal{D}\bar{\psi} \mathcal{D}A_\mu e^{S_G(A) + \bar{\psi} D(A) \psi} \mathcal{O}, \quad (31)$$

where $S_G(A)$ and $\bar{\psi} D(A) \psi$ are the QCD gauge and quark actions, respectively.

By comparing eqs.(26) and (27) we obtain

$$G_{NJ_\mu N}(q, t, \tau) = |Z_N|^2 e^{-E_N(t-\tau)} e^{-E'_N t} \frac{-i\gamma \cdot p + m_N}{2E_N} W_\mu^{\text{even}}(q) \frac{-i\gamma \cdot p' + m_N}{2E'_N}, \quad (32)$$

$$\begin{aligned} G_{NJ_\mu N}^Q(q, t, \tau) = & |Z_N|^2 e^{-E_N(t-\tau)} e^{-E'_N t} \left[\frac{-i\gamma \cdot p + m_N}{2E_N} W_\mu^{\text{odd}}(q) \frac{-i\gamma \cdot p' + m_N}{2E'_N} \right. \\ & + \frac{f_N^1 m_N}{2E_N} \gamma_5 W_\mu^{\text{even}}(q) \frac{-i\gamma \cdot p' + m_N}{2E'_N} \\ & \left. + \frac{-i\gamma \cdot p + m_N}{2E_N} W_\mu^{\text{even}}(q) \frac{f_N^1 m_N}{2E'_N} \gamma_5 \right]. \end{aligned} \quad (33)$$

These formulae are one of the main results of this paper. They show that the parity-even form factor W_μ^{even} multiplied with the parity-odd term f_N^1 of the two-point function has to be removed from the three-point function $G_{NJ_\mu N}^Q$ at order θ , in order to obtain $W_\mu^{\text{odd}}(q)$. We will see in Sec. IV how significant this subtraction is.

C. Extraction of f_N^1 from the nucleon two-point function

In order to determine f_N^1 we consider the two-point function of the nucleon given by

$$\begin{aligned} G_{NN}^\theta(p, t) &\equiv \langle \theta | N(\vec{p}, t) \bar{N}(\vec{p}, 0) | \theta \rangle \\ &= |Z_N^\theta|^2 e^{-E_{N^\theta} t} \frac{-i\gamma \cdot p + m_{N^\theta} e^{if_N(\theta)\gamma_5}}{2E_{N^\theta}} \end{aligned} \quad (34)$$

$$= \langle N(\vec{p}, t) \bar{N}(\vec{p}, 0) e^{i\theta Q} \rangle. \quad (35)$$

By comparing the operator expression (34) with the path integral expression (35) at each order of θ , we obtain

$$G_{NN}(\vec{p}, t) \equiv \langle N(\vec{p}, t) \bar{N}(\vec{p}, 0) \rangle = |Z_N|^2 e^{-E_N t} \frac{-i\gamma \cdot p + m_N}{2E_N} \quad (36)$$

at θ^0 and

$$G_{NN}^Q(\vec{p}, t) \equiv \langle N(\vec{p}, t) \bar{N}(\vec{p}, 0) Q \rangle = |Z_N|^2 e^{-E_N t} \frac{f_N^1 m_N}{2E_N} \gamma_5 \quad (37)$$

at θ^1 . These formulae tell us that f_N^1 can be determined numerically from the nucleon propagators through the appropriate insertion of Q .

III. SIMULATION DETAILS

A. Fermion and gauge actions

For the quark field we employ the domain-wall fermion action[15]:

$$S_F = - \sum_{x,s,x',s'} \bar{\psi}(x,s) D_{\text{DW}}(x,s;x',s') \psi(x',s') + \sum_x m_f \bar{q}(x) q(x), \quad (38)$$

$$D_{\text{DW}}(x,s;x',s') = D^4(x,x') \delta_{s,s'} + \delta_{x,x'} D^5(s,s') + (M-5) \delta_{x,x'} \delta_{s,s'}, \quad (39)$$

$$D^4(x,x') = \sum_{\mu} \frac{1}{2} [(1 - \gamma_{\mu}) U_{\mu}(x) \delta_{x+\hat{\mu},x'} + (1 + \gamma_{\mu}) U_{\mu}^{\dagger}(x') \delta_{x,x'+\hat{\mu}}], \quad (40)$$

$$D^5(s,s') = \begin{cases} \frac{1}{2}(1 - \gamma_5) \delta_{2,s'} & (s=1) \\ \frac{1}{2}(1 - \gamma_5) \delta_{s+1,s'} + \frac{1}{2}(1 + \gamma_5) \delta_{s-1,s'} & (1 < s < N_s) \\ \frac{1}{2}(1 + \gamma_5) \delta_{N_s-1,s'} & (s=N_s) \end{cases} \quad (41)$$

where x, x' are four dimensional space-time coordinates, s, s' are coordinates in the fifth dimension of length N_s , and M is the domain-wall height. Here q, \bar{q} are four dimensional physical quark fields given by

$$q(x) = \frac{1}{2}(1 - \gamma_5) \psi(x, 1) + \frac{1}{2}(1 + \gamma_5) \psi(x, N_s), \quad (42)$$

$$\bar{q}(x) = \bar{\psi}(x, N_s) \frac{1}{2}(1 - \gamma_5) + \bar{\psi}(x, 1) \frac{1}{2}(1 + \gamma_5) \quad (43)$$

and m_f is the bare quark mass. This action has exact chiral symmetry at $N_s \rightarrow \infty$, and therefore it is expected that the fermion fields respond properly to the topological charge of the gauge fields.

For the gauge field we employ the following improved action:

$$S_G = \frac{\beta}{6} \left\{ c_0 \sum_{\text{plaq}} \text{Tr } U_{\text{plaq}} + c_1 \sum_{\text{rect}} \text{Tr } U_{\text{rect}} \right\}, \quad (44)$$

where the first term represents the plaquette and the second the 1×2 rectangle loop. In this paper we take $c_0 = 3.648$ and $c_1 = -0.331$, proposed by Iwasaki using the renormalization group analysis[18]. The action with this parameter choice is called the RG improved gauge action.

B. Topological charge

In continuum QCD, the topological charge density is defined by

$$q(x) = \frac{1}{32\pi^2} \varepsilon_{\mu\nu\alpha\beta} \text{Tr } G_{\mu\nu}(x) G_{\alpha\beta}(x) \quad (45)$$

and the topological charge is given by the integration of $q(x)$ over space-time:

$$Q = \int d^4x q(x). \quad (46)$$

In our lattice calculation we define the topological charge by the improved bosonic form[19], which is given by

$$Q_{\text{imp}} = \sum_x [c_0 Q_{\text{plaq}}(x) + c_1 Q_{\text{rect}}(x)] \quad (47)$$

$$Q_{\text{plaq}} = \frac{1}{32\pi^2} \varepsilon_{\mu\nu\alpha\beta} \text{Tr } (F_{\mu\nu}^P F_{\alpha\beta}^P), \quad Q_{\text{rect}} = \frac{2}{32\pi^2} \varepsilon_{\mu\nu\alpha\beta} \text{Tr } (F_{\mu\nu}^R F_{\alpha\beta}^R) \quad (48)$$

where $F_{\mu\nu}^P$ and $F_{\mu\nu}^R$ are field strengths constructed from the plaquette clover and the rectan-

gular clovers as depicted in Fig. 1. Their explicit expressions are given by

$$\begin{aligned}
F_{\mu\nu}^P(x) = & \frac{\text{Im}}{4} \sum_{x,\mu,\nu} \text{tr} \left[U_\mu(x) U_\nu(x + \hat{\mu}) U_\mu^\dagger(x + \hat{\nu}) U_\nu^\dagger(x) \right. \\
& + U_\nu(x) U_\mu^\dagger(x - \hat{\mu} + \hat{\nu}) U_\nu^\dagger(x - \hat{\mu}) U_\mu(x - \hat{\mu}) \\
& + U_\mu^\dagger(x - \hat{\mu}) U_\nu^\dagger(x - \hat{\mu} - \hat{\nu}) U_\mu(x - \hat{\mu} - \hat{\nu}) U_\nu(x - \hat{\nu}) \\
& \left. + U_\nu^\dagger(x - \hat{\nu}) U_\mu(x - \hat{\nu}) U_\nu(x + \hat{\mu} - \hat{\nu}) U_\mu^\dagger(x) \right], \tag{49}
\end{aligned}$$

$$\begin{aligned}
F_{\mu\nu}^R(x) = & \frac{\text{Im}}{8} \sum_{x,\mu,\nu} \left\{ \text{tr} \left[U_\mu(x) U_\nu(x + \hat{\mu}) U_\nu(x + \hat{\mu} + \hat{\nu}) U_\mu^\dagger(x + 2\hat{\nu}) U_\nu^\dagger(x + \hat{\nu}) U_\nu^\dagger(x) \right. \right. \\
& + U_\nu(x) U_\nu(x + \hat{\nu}) U_\mu^\dagger(x - \hat{\mu} + 2\hat{\nu}) U_\nu^\dagger(x - \hat{\mu} + \hat{\nu}) U_\nu^\dagger(x - \hat{\mu}) U_\mu(x - \hat{\mu}) \\
& + U_\mu^\dagger(x - \hat{\mu}) U_\nu^\dagger(x - \hat{\mu} - \hat{\nu}) U_\nu^\dagger(x - \hat{\mu} - 2\hat{\nu}) U_\mu(x - \hat{\mu} - 2\hat{\nu}) U_\nu(x - 2\hat{\nu}) U_\nu(x - \hat{\nu}) \\
& + U_\nu^\dagger(x - \hat{\nu}) U_\nu^\dagger(x - 2\hat{\nu}) U_\mu(x - 2\hat{\nu}) U_\nu(x + \hat{\mu} - 2\hat{\nu}) U_\nu(x + \hat{\mu} - \hat{\nu}) U_\mu^\dagger(x) \left. \right] \\
& + \text{tr} \left[U_\mu(x) U_\mu(x + \hat{\mu}) U_\nu(x + 2\hat{\mu}) U_\mu^\dagger(x + \hat{\nu} + \hat{\mu}) U_\mu^\dagger(x + \hat{\nu}) U_\nu^\dagger(x) \right. \\
& + U_\nu(x) U_\mu^\dagger(x - \hat{\mu} + \hat{\nu}) U_\mu^\dagger(x - 2\hat{\mu} + \hat{\nu}) U_\nu^\dagger(x - 2\hat{\mu}) U_\mu(x - 2\hat{\mu}) U_\mu(x - \hat{\mu}) \\
& + U_\mu^\dagger(x - \hat{\mu}) U_\mu^\dagger(x - 2\hat{\mu}) U_\nu^\dagger(x - 2\hat{\mu} - \hat{\nu}) U_\mu(x - 2\hat{\mu} - \hat{\nu}) U_\mu(x - \hat{\mu} - \hat{\nu}) U_\nu(x - \hat{\nu}) \\
& \left. + U_\nu^\dagger(x - \hat{\nu}) U_\mu(x - \hat{\nu}) U_\mu(x - \hat{\nu} + \hat{\mu}) U_\nu(x + 2\hat{\mu} - \hat{\nu}) U_\mu^\dagger(x + \hat{\mu}) U_\mu^\dagger(x) \right] \left. \right\}. \tag{50}
\end{aligned}$$

In order to remove $O(a^2)$ discretization errors in Q_{imp} at the tree level, we take $c_1 = -1/12$ and $c_0 = 1 - 8c_1 = 5/3$ [20].

C. Nucleon three-point functions and form factors

To compute nucleon three-point functions, we construct the amplitudes for the six diagrams in Fig.2, each of which consists of two quark propagators and one double quark propagator with an insertion of the electromagnetic current J_μ^{EM} :

$$J_\mu^{\text{EM}}(x) = e^u V_\mu^u(x) + e^d V_\mu^d(x) + e^s V_\mu^s(x) \tag{51}$$

with $V_\mu^i(x)$ ($i = u, d, s$) the conserved vector current of flavor i defined by

$$V_\mu^i(x) = \sum_s j_\mu^i(x, s), \tag{52}$$

$$\begin{aligned}
j_\mu^i(x, s) = & \frac{1}{2} \left[\bar{\psi}^i(x, s) (1 - \gamma_\mu) U_\mu(x) \psi^i(x + \hat{\mu}, s) \right. \\
& \left. + \bar{\psi}^i(x + \hat{\mu}, s) (1 + \gamma_\mu) U_\mu^\dagger(x) \psi^i(x, s) \right]. \tag{53}
\end{aligned}$$

Since this current is conserved, the renormalization factor satisfies $Z_V = 1$. To insert V_μ^i , we use the ordinary source method.

We do not consider the disconnected diagrams depicted in Fig. 3, since this contribution vanishes in the SU(3) flavor symmetric limit due to the fact that $e^u + e^d + e^s = 0$. In future investigations, however, it is necessary to check if this contribution is indeed small or not for $m_{u,d} \neq m_s$.

D. Lattice parameters

We generate quenched gauge configurations on a $16^3 \times 32$ lattice with the RG improved gauge action at $\beta = 2.6$. Gauge configurations separated by 200 sweeps are used for measurements after 2000 sweeps for thermalization, where one sweep consists of one heat-bath update followed by four over-relaxation steps. The quark propagator is calculated using the domain-wall fermion with $N_s = 16$ and $M = 1.8$, where N_s is a size of the fifth dimension and M is the domain-wall height. These parameters are the same as those employed in Ref.[21], in which the lattice spacing was determined to be $a^{-1} = 1.875(56)\text{GeV}$ from the ρ meson mass. The residual quark mass m_{res} , which represents the explicit chiral symmetry breaking effect at finite N_s , is found to be $m_{\text{res}} \simeq 4\text{MeV}$.

We take the bare quark mass $m_{fa} = 0.03$ corresponding to the ratio of pseudoscalar to vector meson masses $m_{PS}/m_V = 0.629(8)$ [21]. To reduce the effects of unwanted excited hadron states, we calculate the quark propagator employing an exponentially smeared source, given by Ae^{-Bra} with $A = 1.28$ and $B = 0.40$, where ra is the distance from the origin at $(7, 7, 7)$ in the lattice unit. We take the periodic boundary condition for both gauge and fermion fields in order to minimize possible violation of the equivalence between the bosonic and the fermionic definitions of topological charge.

In the calculation of three-point functions, the electromagnetic current is inserted at the fixed time slice $\tau = 6$. The nucleon sink is varied as a function of t with the nucleon source fixed at $t = 1$. We move the final state nucleon with one of the three non-zero spatial momenta $\vec{p} = (\pi/8, 0, 0)$, $(0, \pi/8, 0)$, $(0, 0, \pi/8)$, while the initial state nucleon is placed at rest $\vec{p}' = (0, 0, 0)$.

We accumulate 730 configurations for measurements. Errors are estimated by the single elimination jackknife procedure for all measured quantities.

IV. NUMERICAL RESULTS

A. Topological charge

In order to reduce ultra-violet fluctuations of gauge configurations in the calculation of the topological charge, we employ the cooling method using the action in eq.(44) with $c_1 = 3.648$ and $c_0 = -0.331$. In Fig. 4 we show both Q_{plaq} and Q_{imp} as a function of the cooling steps, where Q_{plaq} is the naive plaquette definition of the topological charge and Q_{imp} is the improved one in eq.(47). It is clearly observed that Q_{imp} approach integer values much faster than Q_{plaq} as the cooling step increases. The values after 20 cooling steps are also closer to integer values. The deviation from integer is within a few percent for Q_{imp} after 20 cooling steps. As the topological charge, we employ Q_{imp} measured after 20 cooling steps on each configuration.

In Fig. 5 we show the time history of the topological charge as a function of the gauge configuration separated by 200 sweeps, where we do not recognize any long autocorrelation. In addition, the histogram of the topological charge in Fig. 6 exhibits nearly a Gaussian distribution. These observations suggest that the sampling of the topological charge is sufficiently good in our calculation.

B. Nucleon propagator

1. $O(\theta^0)$ contribution

From the analysis in Sec. IIC, the $O(\theta^0)$ contribution of the nucleon propagator should behave as

$$\text{tr} [G_{NN}(\vec{p}, t)\Gamma_4] = \begin{cases} |Z_N|^2 e^{-m_N t} + \dots & (|\vec{p}| = 0) \\ |Z_N(p)|^2 \frac{m_N}{E_N} e^{-E_N t} + \dots & (|\vec{p}| = 1) \end{cases}, \quad (54)$$

where $\Gamma_4 = (1 + \gamma_4)/2$ and the dots represent the contribution from the excited states. Here $|\vec{p}| = 1$ is a shorthand notation of $\vec{p} = (\pi/8)\vec{n}$ with $|\vec{n}| = 1$.

The nucleon propagators from the smeared source and the point sink with $|\vec{p}| = 0$ and $|\vec{p}| = 1$ are plotted in Fig. 7, and the corresponding effective masses are given in Fig.8.

Choosing $9 \leq t \leq 13$ for the fitting range, we obtain

$$\begin{aligned} E_N a &= \begin{cases} 0.7114(43) & (|\vec{p}| = 0) \\ 0.8068(77) & (|\vec{p}| = 1) \end{cases}, \\ Z_N &= \begin{cases} 2162(87) & (|\vec{p}| = 0) \\ 1453(104) & (|\vec{p}| = 1) \end{cases}. \end{aligned} \quad (55)$$

Note that $E_N a = 0.8068(77)$ at $|\vec{p}| = 1$ agrees with the relativistic dispersion relation $\sqrt{(m_N a)^2 + (\pi/8)^2} = 0.813(4)$ within the error.

2. $O(\theta^1)$ contribution and the determination of f_N^1

In Sec. II C we have shown that the parity-odd part of the nucleon propagator should have the following form at the order of θ^1 :

$$\text{tr} [G_{NN}^Q(0, t) \frac{\gamma_5}{2}] = |Z_N|^2 f_N^1 e^{-m_N t}, \quad (56)$$

$$\text{tr} [G_{NN}^Q(p, t) \frac{\gamma_5}{2}] = |Z_N(p)|^2 \frac{m_N}{E_N} f_N^1 e^{-E_N t}. \quad (57)$$

In Fig.9 we plot the parity-odd part with the insertion of Q , while the parity-even part without Q , $\text{tr} [G_{NN}(p, t) \frac{\gamma_5}{2}]$, is given in Fig.10 for comparison. The latter vanishes at all time slices as expected. On the other hand, the former is non-zero, showing an exponential fall-off at large t . After averaging over the forward and backward propagators in time, we fit the parity-odd part at $9 \leq t \leq 14$, by the form $\xi e^{-E_N t}$ with E_N fixed to the value obtained from the previous fit of the $O(\theta^0)$ contribution. The fit, represented by the solid line in Fig. 9, is reasonably good, showing that the decay rate of the parity-odd part is consistent with that of the parity-even part for both $|\vec{p}| = 0$ and 1. Note however that the small deviation indicates that the present statistics are still insufficient at large t for $|\vec{p}| = 1$.

Another confirmation of consistency is found in the effective mass plot of Fig. 11, where the parity-odd part of the nucleon propagator with Q and the parity-even part without Q are compared.

With the aid of E_N and Z_N obtained previously, ξ is converted to f_N^1 as

$$f_N^1 = \begin{cases} -0.247(17) & (|\vec{p}| = 0) \\ -0.243(20) & (|\vec{p}| = 1) \end{cases}. \quad (58)$$

Despite the deviation at large t for $|\vec{p}| = 1$, the two estimates of f_N^1 agree within the errors. In our analysis we will use f_N^1 obtained from $|\vec{p}| = 0$.

We note that the exponential fall-off of G_{NN}^Q is very sensitive to the distribution of the topological charge. One could use this quantity to judge whether the sampling of the topological charge is sufficiently good: if the exponential fall-off of G_{NN}^Q does not agree with that of G_{NN} , the sampling is not satisfactory.

C. Form factors

1. Extraction from three-point functions

In order to remove the exponential fall-off due to the nucleon propagation in the three-point functions, we divide them by the two-point function $G_{NN}(\vec{p}, t)$ with the smeared source at $t = 1$ and the point sink at t :

$$\Pi_\mu^e(q; t, \tau) = \frac{G_{NJ_\mu N}(q; t, \tau)}{G_{NN}(q, t)} R(q; \tau, t), \quad (59)$$

$$\Pi_\mu^o(q; t, \tau) = \frac{G_{NJ_\mu N}^Q(q; t, \tau)}{G_{NN}(q, t)} R(q; \tau, t) \quad (60)$$

with

$$R(q; \tau, t) = \left[\frac{G_{NN}(q, t) G_{NN}(q, \tau) G_{NN}^{PP}(0, t - \tau)}{G_{NN}(0, t) G_{NN}(0, \tau) G_{NN}^{PP}(q, t - \tau)} \right]^{1/2}, \quad (61)$$

where the factor R is to remove the interpolating field dependent normalization factors. Here we introduce a new two-point function $G_{NN}^{PP}(q, t)$ that has the point source at $t = 1$ and the point sink at t , and $G_{NN}^{PP}(q, t - \tau)$ represents that the source point is started at $t = \tau$. In Fig. 12 we plot the t dependence of $R(q; \tau, t)$ with $\tau = 6$ and $|\vec{q}| = 1$. As we expect, the correction factor R is independent of t in the large t region.

The form factors are extracted from the ratios defined in eqs.(59) and (60) by applying appropriate projections of gamma matrices. From the $O(\theta^0)$ contribution $\Pi_4^e(q; t, \tau)$ of eq.(59), F_1 and F_2 can be extracted as

$$\text{tr} [\Pi_4^e(q; t, \tau) \Gamma_4] = \frac{E_N + m_N}{E_N} \left(F_1(q^2) + F_2(q^2) \frac{q^2}{4m_N^2} \right), \quad (62)$$

$$\text{tr} [\Pi_i^e(q; t, \tau) i\Gamma_4 \gamma_5 \gamma_j] = \varepsilon_{ijk} \frac{q_k}{E_N} (F_1(q^2) + F_2(q^2)), \quad (63)$$

where we use eq.(32). The F_1 and F_2 are related to the electric (G_e) and the magnetic (G_m) form factors as

$$G_e(q^2) = F_1(q^2) + F_2(q^2) \frac{q^2}{4m_N^2}, \quad (64)$$

$$G_m(q^2) = F_1(q^2) + F_2(q^2). \quad (65)$$

These quantities become the electric charge and the magnetic moment at $q^2 \rightarrow 0$. Therefore $G_e(0) = 0(1)$ and $G_m(0) = -1.91(2.79)[22]$ for the neutron(proton).

We can extract the form factor $F_3(q^2)$, which is relevant to the electric dipole moment, in two different ways from $\Pi_4^o(q; t, \tau)$ of eq.(60):

$$\begin{aligned} \text{tr} [\Pi_4^o(q, t, \tau) \Gamma_4 \gamma_5] &= \frac{\vec{q}^2}{2E_N m_N} F_3(q^2) \\ &+ \left[\frac{E_N + m_N}{2E_N} F_1(q^2) + \frac{\vec{q}^2}{4m_N E_N} F_2(q^2) \right] f_N^1, \end{aligned} \quad (66)$$

$$\begin{aligned} \text{tr} [\Pi_4^o(q, t, \tau) i \Gamma_4 \gamma_5 \gamma_i] &= -\frac{E_N + m_N}{2E_N m_N} q_i F_3(q^2) \\ &+ \left[-\frac{q_i}{2E_N} F_1(q^2) - \frac{q_i(E_N + 3m_N)}{4m_N E_N} F_2(q^2) \right] f_N^1, \end{aligned} \quad (67)$$

where we use eq.(33). It will be clear that the consistency between the two different extractions of $F_3(q^2)$ provides a crucial test for the validity of actual calculations.

2. Parity-even part

We first consider the parity-even part of the form factor. In Figs. 13 and 14 we show the magnetic and electric form factors obtained from eqs.(62) and (63). We observe good plateaux except for the electric form factor of the neutron. Employing a constant fit with $10 \leq t \leq 14$ for G_m and $12 \leq t \leq 15$ for G_e we obtain

$$G_m(q^2) = \begin{cases} -0.591(37) & (\text{neutron}) \\ 0.952(60) & (\text{proton}) \end{cases} \quad (68)$$

$$G_e(q^2) = 0.502(33) \quad (\text{proton}) \quad (69)$$

at $q^2 = 0.58 \text{ GeV}^2$. Here the value for G_e^n is not quoted since it is difficult to find a plateau for the fit. Note also that the value of G_e slightly depends on the fitting range, as could be seen from the figure. These values are compared with the previous lattice result[23] obtained at a similar nucleon mass and lattice spacing using the nonperturbatively $O(a)$ improved

Wilson quark and the plaquette gauge actions: $G_m(q^2) = -0.73(4)$ for the neutron, and $G_m(q^2) = 1.17(6)$ and $G_e(q^2) = 0.451(13)$ for the proton.

Experimentally the proton electromagnetic form factors at small q^2 have been measured as[24],

$$G_m^{p(\text{exp})}(q^2 = 0.58\text{GeV}^2) = 0.848 \pm 0.011, \quad G_e^{p(\text{exp})}(q^2 = 0.58\text{GeV}^2) = 0.294 \pm 0.008. \quad (70)$$

Recent experimental measurements for neutron form factors cover a wide range of q^2 from very small $q^2 \sim 0.3 \text{ GeV}^2$ to more than 1 GeV^2 with high precision[25]. For example, the neutron magnetic form factor at $q^2 = 0.6 \text{ GeV}^2$ is measured as[26]

$$G_m^{n(\text{exp})}(q^2 = 0.6\text{GeV}^2) = -0.568 \pm 0.007(\text{stat.}) \pm 0.015(\text{syst.}), \quad (71)$$

and the electric form factor at $q^2 = 0.5 \text{ GeV}^2$ is[27]

$$G_e^{n(\text{exp})}(q^2 = 0.5\text{GeV}^2) = 0.0463 \pm 0.0062(\text{stat.}) \pm 0.0034(\text{syst.}). \quad (72)$$

The fact that our results are not so much different from these experimental values may suggest that systematic errors involved in our calculations, such as the large quark mass, the small lattice size, the non-zero lattice spacing and the quenching, are not so large on these quantities.

The form factors F_1 and F_2 are obtained from G_m and G_e using eqs.(64) and (65). We show the time dependence of F_1 and F_2 in Figs. 15 and 16. We observe plateaus at $t \geq 13$ for $F_2^{n,p}$ and F_1^p but not for F_1^n , which behaves badly as G_e^n does. We think that this behavior is caused by the contribution from other excited states, as pointed out in Ref.[28]. Therefore we have tried to include the contributions of the parity-odd nucleon state N_- in our analysis, using the formulae given in Appendix A. Although larger errors prevent us from extracting the reliable values for G_e^n and F_1^n , we find a much better plateau for G_e^n as shown in Fig. 17 and for F_1^n in Fig. 18.

Applying a constant fit to F_1^p and $F_2^{n,p}$ with $13 \leq t \leq 16$, we obtain

$$F_1^p(q^2) = 0.515(37), \quad F_2^n(q^2) = -0.560(40), \quad F_2^p(q^2) = 0.399(37), \quad (73)$$

which are compared with $F_1^p(q^2) = 0.499(13)$, $F_2^p(q^2) = 0.68(6)$ from Ref.[23].

3. Parity-odd part

We now consider the main target of our calculation: the parity-odd part of the form factors. Substituting $G_{NJ_\mu N}^Q(q; t, \tau)$, $F_1(q^2)$, $F_2(q^2)$ and f_N^1 into eqs.(66) and (67), we extract the form factor $F_3(q^2)$ in two different ways. We first plot $\text{tr}[\Pi_4^o(q, t, \tau)\Gamma_4\gamma_5]$ and $\text{tr}[\Pi_4^o(q, t, \tau)\Gamma_4\gamma_5\gamma_i]$ in Figs. 19 for the nucleon and in 20 for the proton, together with the second terms in the right hand side of eqs.(66) and (67), composed of F_1 , F_2 and f_N^1 . Comparing the two extractions, we find that $\text{tr}[\Pi_4^o(q, t, \tau)\Gamma_4\gamma_5]$ and $\text{tr}[\Pi_4^o(q, t, \tau)\Gamma_4\gamma_5\gamma_i]$ shown by open symbols do not agree with each other. In particular, for the case of the proton, $\text{tr}[\Pi_4^o(q, t, \tau)\Gamma_4\gamma_5]$ is very large, while $\text{tr}[\Pi_4^o(q, t, \tau)\Gamma_4\gamma_5\gamma_i]$ is almost zero.

We note that $\text{tr}[\Pi_4^o(q, t, \tau)\Gamma_4\gamma_5]$ and $\text{tr}[\Pi_4^o(q, t, \tau)\Gamma_4\gamma_5\gamma_i]$ are almost zero for the neutron is consistent with the previous result[13], in which the contribution of the mixing term was not considered.

Figure 21 shows the result after subtracting the second terms from $\text{tr}[\Pi_4^o(q, t, \tau)\Gamma_4\gamma_5]$ (circles) and $\text{tr}[\Pi_4^o(q, t, \tau)\Gamma_4\gamma_5\gamma_i]$ (triangles) for the neutron (top panel) and the proton (bottom panel). It is gratifying to observe that the two ways of projections give values of F_3 consistent with each other. In particular, the significant difference between the two projections for the proton almost vanishes after removing the second terms.

Making a constant fit to the result of eq.(67) over $12 \leq t \leq 15$, we obtain

$$\frac{1}{2m_N}F_3(q^2 \simeq 0.58 \text{ GeV}^2) = \begin{cases} -0.024(5) \text{ e} \cdot \text{fm} & (\text{neutron}) \\ 0.021(6) \text{ e} \cdot \text{fm} & (\text{proton}) \end{cases} \quad (74)$$

with $a^{-1} = 1.875(56)\text{GeV}$ [21]. Note that the opposite sign between neutron and proton is consistent with the estimate of Ref.[8], where the baryon EDM is proportional to its magnetic moment. It should be remembered that our values are obtained at a non-zero q^2 . With the same caution in mind, our result may be compared with other estimates of $F_3(0)/2m_N$: $3.6 \times 10^{-3} \text{ e} \cdot \text{fm}$ [4], $7.5 \pm 3.2 \times 10^{-3} \text{ e} \cdot \text{fm}$ [8] and $3.9 \times 10^{-3} \text{ e} \cdot \text{fm}$ [5].

V. CONCLUSION AND DISCUSSION

In this paper we have carried out a feasibility study for the lattice QCD calculation of the neutron electric dipole moment in the presence of the θ term. We took the strategy to extract the nucleon EDM from the nucleon electromagnetic form factor at small θ . We

explained how one could extract the parity-odd part of the form factors, which becomes EDM at zero momentum transfer, from the relevant correlation functions for small θ . We have pointed out that the contribution of the parity-even form factors multiplied by the parity-odd part of the nucleon two-point function has to be subtracted from the parity odd three-point function. We have derived the formula to carry out this subtraction, which is one of the main results.

In the second half, we applied our formula to an actual lattice QCD calculation, employing the domain-wall quark action with the RG improved gauge action in quenched QCD. We used a $16^3 \times 32 \times 16$ lattice at $a^{-1} = 1.875(56)\text{GeV}$ with the quark mass of $m_f = 0.03$, which corresponds to $m_\pi/m_\rho = 0.629(8)$. In order to obtain a sufficient sampling of topological charges, we accumulated 730 configurations, which enabled us to extract the parity-odd part both in the nucleon two- and three-point functions. We have shown that two different γ matrix projections yield values for F_3 consistent with each other, if the subtractions mentioned above are made.

Our lattice calculation gives

$$\frac{1}{2m_N}F_3(q^2 \simeq 0.58 \text{ GeV}^2) = \begin{cases} -0.024(5) \text{ e} \cdot \text{fm} & (\text{neutron}) \\ 0.021(6) \text{ e} \cdot \text{fm} & (\text{proton}) \end{cases}. \quad (75)$$

at $m_f a = 0.03$. In order to obtain the physical value of NEDM, we have to perform various extrapolations: $q^2 \rightarrow 0$ extrapolation, the chiral extrapolation ($m_f \rightarrow m_{\text{phys}}$) and the continuum extrapolation ($a \rightarrow 0$). In addition, we have to remove the quenching error in NEDM, since NEDM vanishes at zero quark mass in QCD but it does not in quenched QCD. While it would be possible to remove each of these systematic errors step by step using the method proposed in this paper, we are now looking for better alternatives with which we can remove them more easily.

Acknowledgments

S. A. would like to thank Prof. A. Kronfeld for useful discussion, which leads to the simpler derivation of eq.(20). We thank Prof. M. Fukugita for his valuable comments on the manuscript. This work is supported in part by Grants-in-Aid of the Ministry of Education (Nos. 12640253, 13640259, 13640260, 14046202, 15204015, 15540251, 15540279, 15740134,

15740165, 16028201, 16540228, 17540249). The numerical simulations have been carried out on the parallel computer CP-PACS.

APPENDIX A: N_+ TO N_- FORM FACTOR

If we include the electromagnetic transistion from N_+ to N_- , eqs.(62) and (63) are modified as

$$\begin{aligned} \text{tr} [\Pi_4^e(q; t, \tau) \Gamma_4] &= \frac{E_N + m_N}{E_N} \left(F_1(q^2) + F_2(q^2) \frac{q^2}{4m_N^2} \right) \\ &+ \left[\frac{\tilde{q}^2}{E_{N_-}(m_N + m_{N_-})} F_3^{N_+ \rightarrow N_-}(q^2) \right. \\ &+ \left. \frac{\tilde{q}^2(E_{N_-} - m_{N_-})(1 - \Lambda)}{E_{N_-}} F_A^{N_+ \rightarrow N_-}(\tilde{q}^2) \right] \Delta_{+-}(t, \tau), \end{aligned} \quad (\text{A1})$$

$$\begin{aligned} \text{tr} [\Pi_i^e(q; t, \tau) i\Gamma_4 \gamma_5 \gamma_j] &= \varepsilon_{ijk} \frac{q_k}{E_N} (F_1(q^2) + F_2(q^2)) \\ &+ \varepsilon_{ijk} \left[-\frac{q_k(m_N - m_{N_-})}{E_{N_-}(m_N + m_{N_-})} F_3^{N_+ \rightarrow N_-}(\tilde{q}^2) \right. \\ &+ \left. \frac{q_k \tilde{q}^2}{E_{N_-}} F_A^{N_+ \rightarrow N_-}(\tilde{q}^2) \right] \Delta_{+-}(t, \tau), \end{aligned} \quad (\text{A2})$$

where

$$\Lambda = \frac{(m_N + m_{N_-})(E_{N_-} - m_N)}{-(E_{N_-} - m_N)^2 + \tilde{q}^2}, \quad \Delta_{+-}(t, \tau) = \frac{(Z_-)^* Z_+}{|Z_+|^2} e^{-(E_{N_-} - E_N)(t - \tau)} \quad (\text{A3})$$

and m_{N_-} is the parity-odd nucleon mass and $F_3^{N_+ \rightarrow N_-}(\tilde{q}^2)$ and $F_A^{N_+ \rightarrow N_-}(\tilde{q}^2)$ are the N_+ to N_- transition form factors with $\tilde{q}^2 = -(E_{N_-} - m_N)^2 + q^2$. $Z_{N_-}(p)$ is the parity-odd nucleon amplitude which can be determined from the N_- propagator. In order to obtain these form

factors we have to consider additional projection formula as follows:

$$\begin{aligned} \text{tr} [\Pi_4^e(q; t, \tau) i\Gamma_4 \gamma_j] &= \frac{q_j}{E_N} \left(F_1(q^2) + \frac{q^2}{2m_N} F_2(q^2) \right) \\ &+ \left[\frac{q_j(E_{N_-} + m_{N_-})}{E_{N_-}(m_N + m_{N_-})} F_3^{N_+ \rightarrow N_-}(\tilde{q}^2) \right. \\ &\left. + \frac{q_j \tilde{q}^2}{E_{N_-}} (1 - \Lambda) F_A^{N_+ \rightarrow N_-}(\tilde{q}^2) \right] \Delta_{+-}(t, \tau), \end{aligned} \quad (\text{A4})$$

$$\begin{aligned} \text{tr} [\Pi_i^e(q; t, \tau) i\Gamma_4] &= \frac{q_i}{E_N} F_1(q^2) - \frac{q_i(E_N - m_N)}{2m_N E_N} F_2(q^2) \\ &+ \left[\frac{q_i(E_{N_-} - m_N)}{(m_N + m_{N_-}) E_{N_-}} F_3^{N_+ \rightarrow N_-}(\tilde{q}^2) \right. \\ &\left. - \frac{q_i \tilde{q}^2 (E_{N_-} - m_N + (-E_{N_-} + m_{N_-}) \Lambda)}{E_{N_-} (E_{N_-} - m_N)} F_A^{N_+ \rightarrow N_-}(\tilde{q}^2) \right] \Delta_{+-}(t, \tau), \end{aligned} \quad (\text{A5})$$

$$\begin{aligned} \text{tr} [\Pi_i^e(q; t, \tau) \Gamma_4 \gamma_j] &= \frac{-E_N + m_N}{E_N} \delta_{ij} F_1(q^2) + \frac{(E_N - m_N)^2 \delta_{ij} - \tilde{q}^2 \delta_{ij} + q_i q_j}{2E_N m_N} F_2(q^2) \\ &- \left[\frac{(E_{N_-} + m_{N_-})(E_{N_-} - m_N) \delta_{ij} - \tilde{q}^2 \delta_{ij} + q_i q_j}{(m_N + m_{N_-}) E_{N_-}} F_3^{N_+ \rightarrow N_-}(\tilde{q}^2) \right. \\ &\left. + \frac{\tilde{q}^2}{E_{N_-}} \left(-(E_{N_-} + m_{N_-}) \delta_{ij} + \frac{\Lambda q_i q_j}{E_{N_-} - m_N} \right) F_A^{N_+ \rightarrow N_-}(\tilde{q}^2) \right] \Delta_{+-}(t, \tau). \end{aligned} \quad (\text{A6})$$

Employing four equations out of the above five formula we can determine F_1 , F_2 , $F_3^{N_+ \rightarrow N_-}$ and $F_A^{N_+ \rightarrow N_-}$. The form factors F_1 and F_2 plotted in Figs. 17 and 18. are obtained with the use of eqs.(A4), (A5) and (A6) ($i = j$ and $i \neq j$).

In Fig. 22 we show the effective mass plot for the parity-odd nucleon. As for $|\vec{p}| = 1$ we have subtracted the N_+ contribution from $\text{tr} [G_{NN}(t, p) \bar{\Gamma}_4]$ with $\bar{\Gamma}_4 = \frac{1-\gamma_4}{2}$, in order to obtain the energy E_{N_-} for the parity-odd state. The global fit with $4 \leq t \leq 9$ for m_{N_-} and $6 \leq t \leq 11$ for E_{N_-} gives

$$m_{N_-} a = 1.017(8), E_{N_-} a = 1.056(18), \quad (\text{A7})$$

where $E_{N_-} a$ is close to the value expected from the relativistic dispersion relation $\sqrt{(m_{N_-} a)^2 + (\pi/8)^2} = 1.090(8)$.

[1] P. G. Harris et al., Phys. Rev. Lett. **82**, 904 (1999).

- [2] V. F. Dmitriev, R. A. Sen'kov, Phys. Rev. Lett. **91**, 212303 (2003).
- [3] M. V. Romalis, W. C. Griffith, J. P. Jacobs, E. N. Fortson, Phys. Rev. Lett. **86**, 2505 (2001).
- [4] R. J. Crewther, P. Di Vecchia, G. Veneziano, E. Witten, Phys. Lett. **B88**, 123 (1979); erratum, *ibid.* **B91**, 487 (1980).
- [5] P. Di Vecchia, Acta Phys. Austriaca Suppl. **22**, 341 (1980).
- [6] R. D. Peccei, H. R. Quinn, Phys. Rev. Lett. **38**, 1440 (1977); R. D. Peccei, Adv. Ser. Direct. High Energy Phys. 3, 503-551 (1989).
- [7] M. Pospelov, A. Ritz, Nucl. Phys. **B558**, 243 (1999); Nucl. Phys. **B573**, 177 (2000); Chuan-Tsung Chan, E. M. Henley, T. Meissner, hep-ph/9905317; M. Pospelov, A. Ritz, Phys. Rev. Lett. **27**, 2526 (1999); Phys. Rev. **D63**, 073015 (2001).
- [8] B. Borasoy, Phys. Rev. **D61**, 114017 (2000).
- [9] S. Aoki, A. Gocksch, Phys. Rev. Lett. **63**, 1125 (1989); erratum, *ibid.* **65**, 1172 (1990).
- [10] S. Aoki, A. Gocksch, A. V. Manohar, S. R. Sharpe, Phys. Rev. Lett. **65**, 1092 (1990).
- [11] D. Guadagnoli, V. Lubicz, G. Martinelli, S. Simula, JHEP **0304**, 019 (2003).
- [12] P. Faccioli, D. Guadagnoli, S. Simula, Phys. Rev. **D70**, 074017 (2004).
- [13] F. Berruto, T. Blum, K. Orginos, A. Soni, Nucl. Phys. Proc. Suppl. 140, 411 (2005).
- [14] S. Aoki, T. Hatsuda, Phys. Rev. **D45**, 2427 (1992).
- [15] D. B. Kaplan, Phys. Lett. **B288**, 342 (1992); Y. Shamir, Nucl. Phys. **B406**, 90 (1993); V. Furman, Y. Shamir, Nucl. Phys. **B439**, 54 (1995).
- [16] R. Narayanan, H. Neuberger, Nucl. Phys. **B443**, 305 (1995); H. Neuberger, Phys. Lett. **B417**, 141 (1998); H. Neuberger, Phys. Lett. **B427**, 353 (1998); H. Neuberger, Phys. Rev. **D57**, 5417 (1998).
- [17] CP-PACS Collaboration, A. Ali Khan *et al.*, Phys. Rev. **D63**, 114504 (2001).
- [18] Y. Iwasaki, Nucl. Phys. **B258**, 148 (1985).
- [19] CP-PACS Collaboration, A. Ali Khan *et al.*, Phys. Rev. **D64**, 114501 (2001).
- [20] P. Weisz, Nucl. Phys. **B212**, 1 (1983); P. Weisz, R. Wohlert, Nucl. Phys. **B236**, 397 (1984); erratum, *ibid.* **B247**, 544 (1984); M. Lüscher, P. Weisz, Commun. Math. Phys. **97**, 59 (1985); erratum, *ibid.* **98**, 433 (1985).
- [21] CP-PACS Collaboration, A. Ali Khan *et al.*, Phys. Rev. **D64**, 114506 (2001).
- [22] S. Eidelman *et al.*, Phys. Lett. **B592**, 1 (2004).
- [23] M. Göckeler *et al.*, Phys. Rev. **D71**, 034508 (2005).

- [24] L. E. Price, *et al.*, Phys. Rev. **D4**, 45 (1971).
- [25] H.-Y. Gao, Int. J. Mod. Phys. **E12**, 1 (2003).
- [26] W. Xu, *et al.*, Phys. Rev. **C67**, R012201 (2003).
- [27] H.Zhu, *et al.*, Phys. Rev. Lett. **87**, 081801 (2001).
- [28] A. Tang, W. Wilcox, R. Lewis, Phys. Rev. **D68**, 094503 (2003).

FIGURES

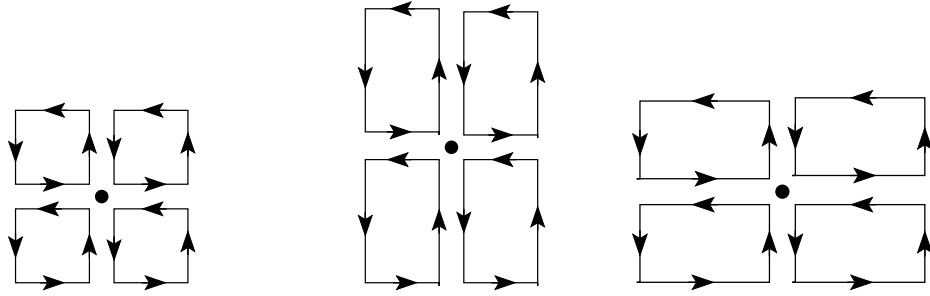
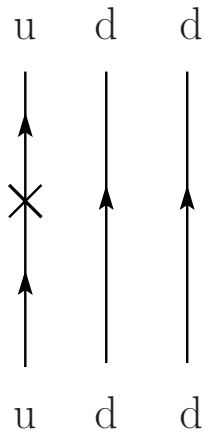
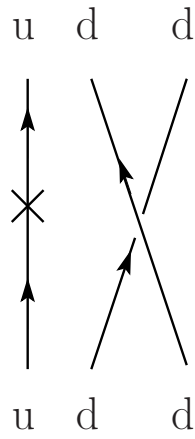


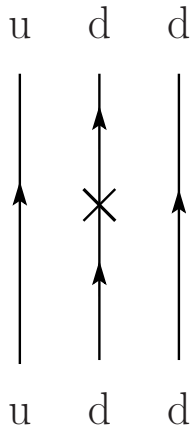
FIG. 1: Plaquette clover (left) and rectangular clovers (middle and right).



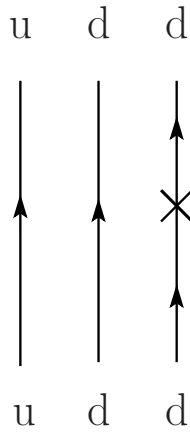
(a)



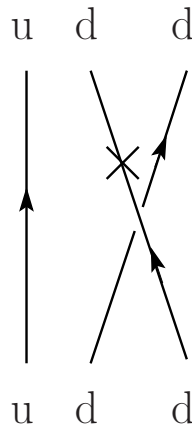
(b)



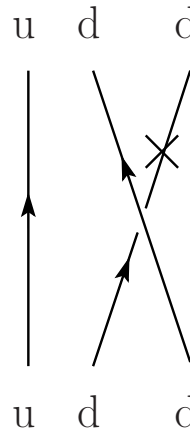
(c)



(d)



(e)



(f)

FIG. 2: Six diagrams contributed to the neutron three-point function. Cross symbol represents the current insertion. In (a), (b) EM current is connected with u quark line, and in (c) \sim (f) with d quark line.

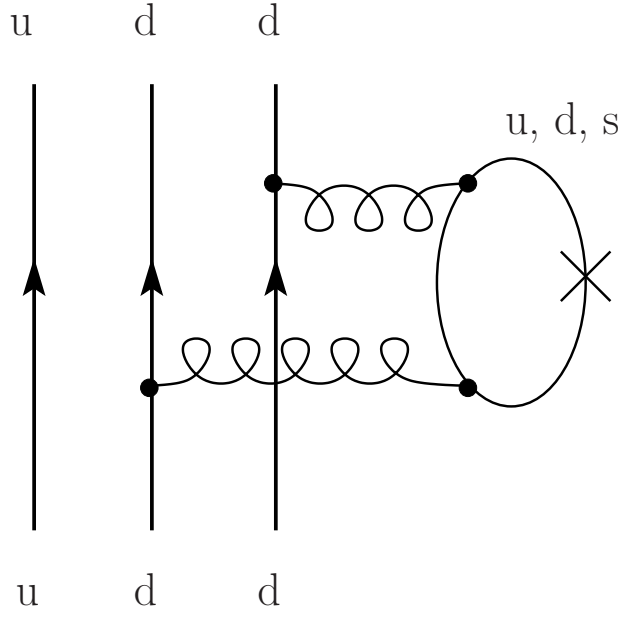


FIG. 3: An example for the disconnected contribution to three-point function. The loop contains u, d, s quarks

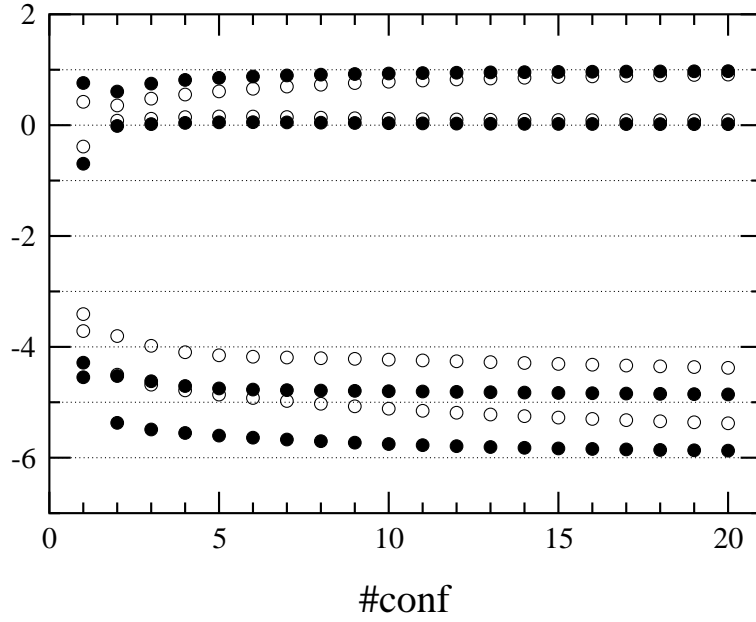


FIG. 4: Topological charge as a function of the number of cooling steps. Open symbols represent the naive plaquette definition and solid symbols the improved definition.

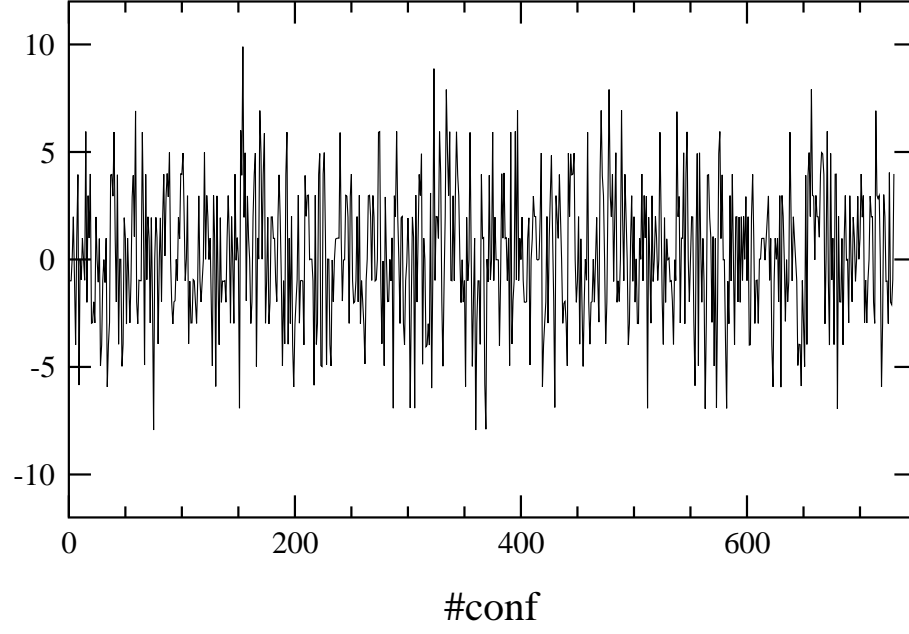


FIG. 5: Time history of the topological charge. Gauge configurations are separated by 200 sweeps.

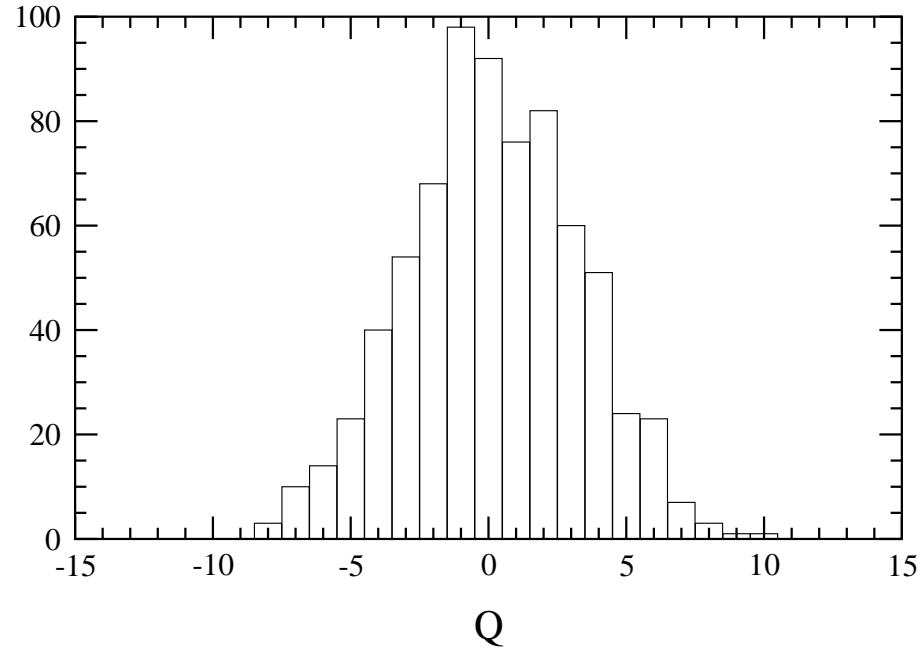


FIG. 6: Histogram of the topological charge.

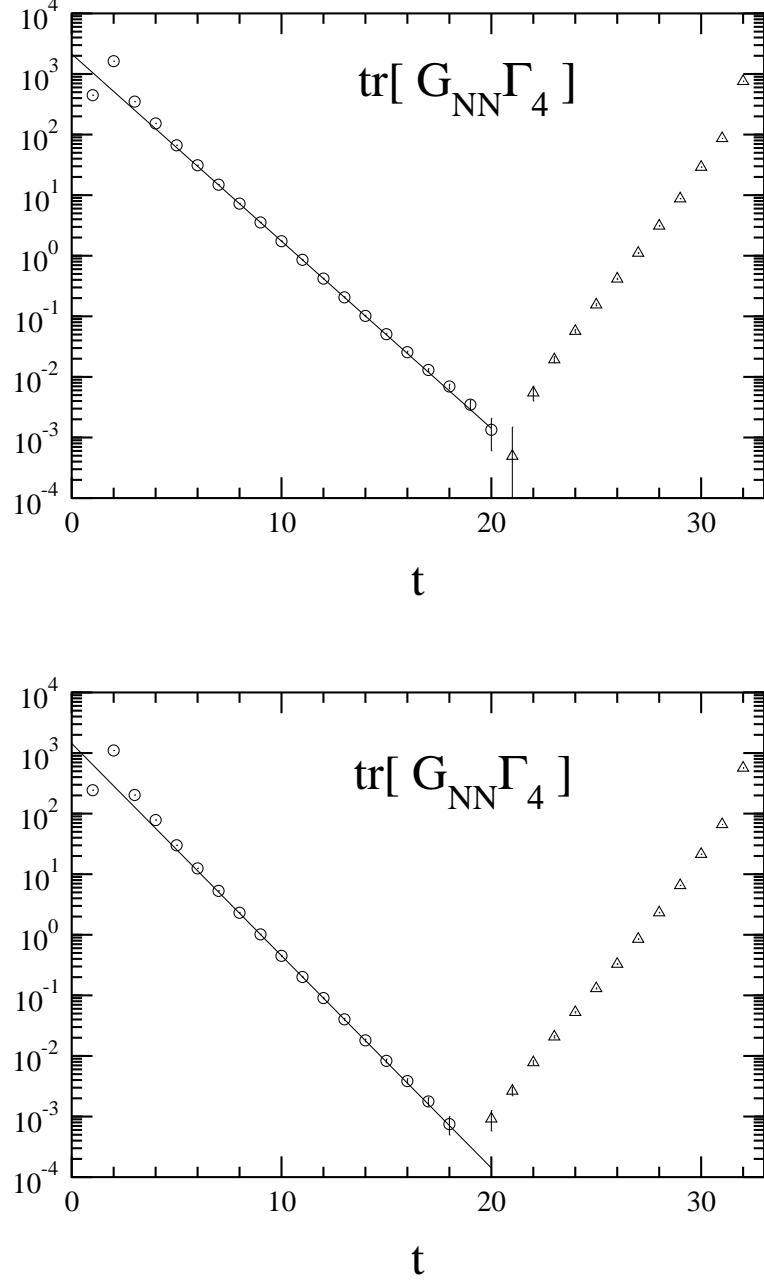


FIG. 7: $\text{tr}[G_{NN}(\vec{p}, t)\Gamma_4]$, $O(\theta^0)$ contribution of the nucleon propagator with Γ_4 projection for $|\vec{p}| = 0$ (top) and $|\vec{p}| = 1$ (bottom). Solid lines denote the fitting results. The parity-odd state dominates the backward propagation in t denoted by triangles.

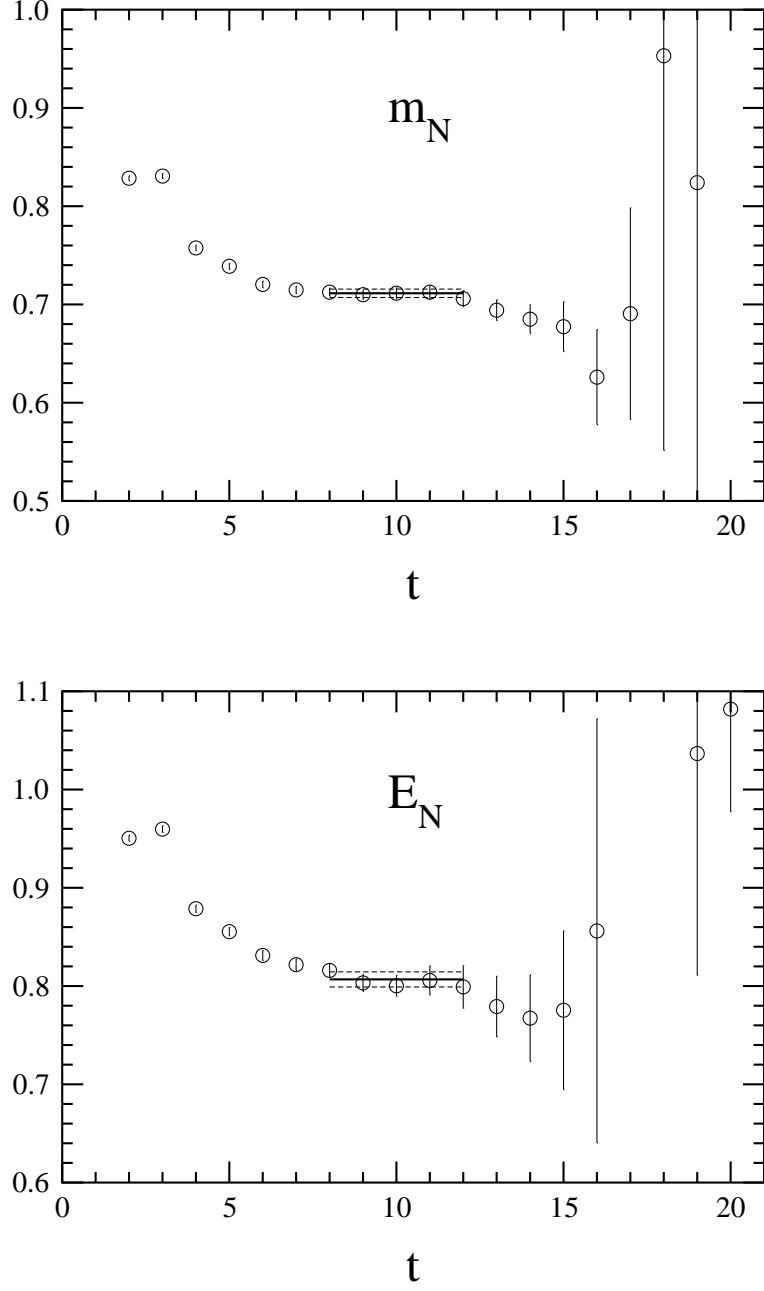


FIG. 8: Effective mass plot for the nucleon with $|\vec{p}^\dagger| = 0$ (top) and $|\vec{p}^\dagger| = 1$ (bottom). Solid(dotted) lines denote the central values(errors) of the global fit.

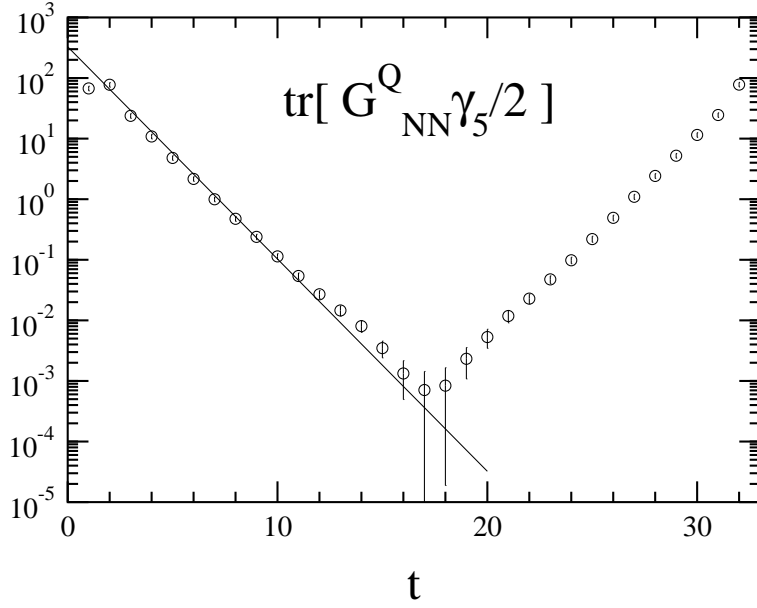
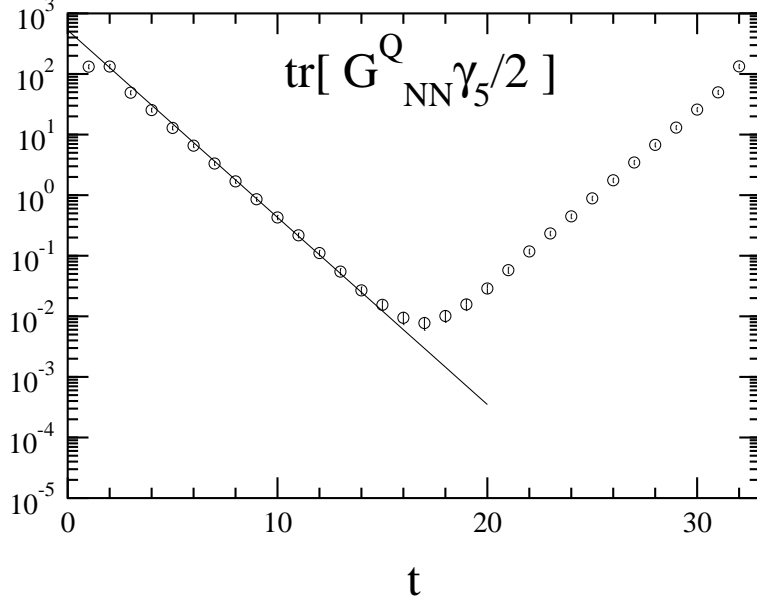


FIG. 9: $\text{tr} \left[G_{NN}^Q(\vec{p}, t) \frac{\gamma_5}{2} \right]$, parity odd part of the nucleon propagator with Q for eq.(56) $|\vec{p}| = 0$ (top) and eq.(57) $|\vec{p}| = 1$ (bottom). The sign of propagator is negative. Solid lines denote the fitting results.

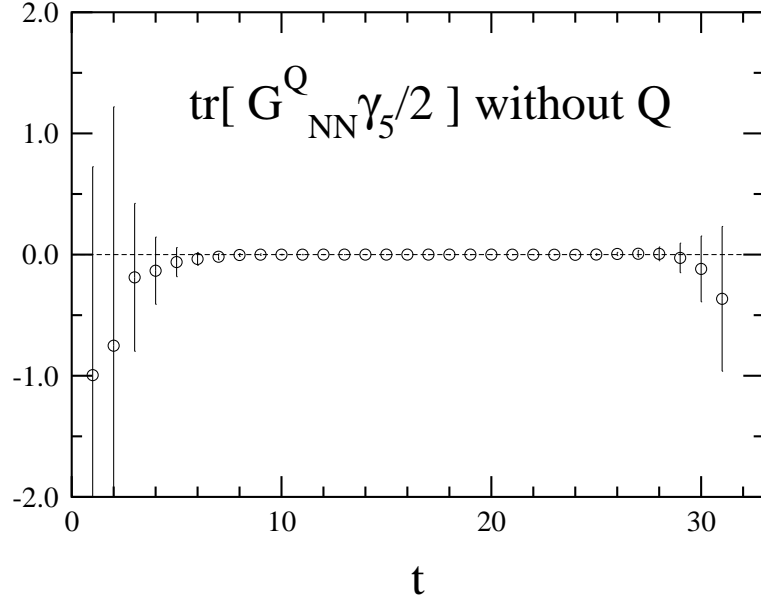
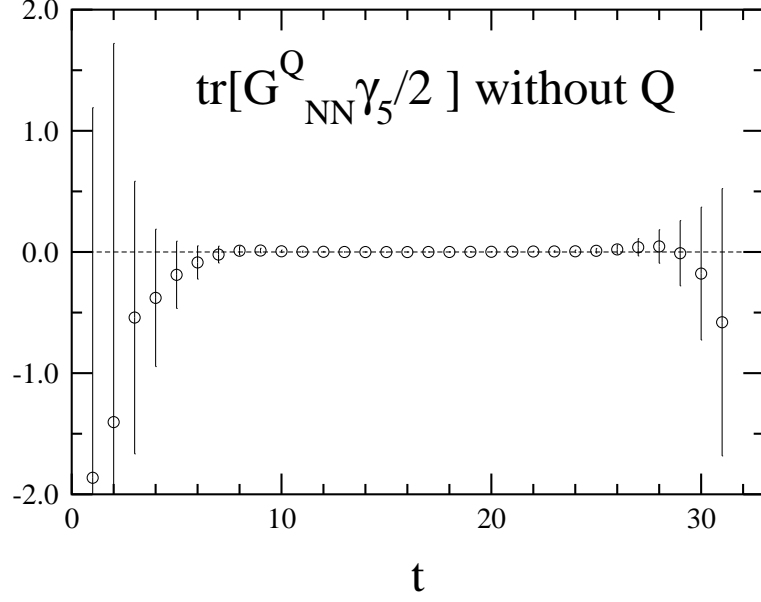


FIG. 10: $\text{tr} [G_{NN}(\vec{p}, t) \frac{\gamma_5}{2}]$, parity odd part of the nucleon propagator without Q for eq.(56) $|\vec{p}| = 0$ (top) and eq.(57) $|\vec{p}| = 1$ (bottom).

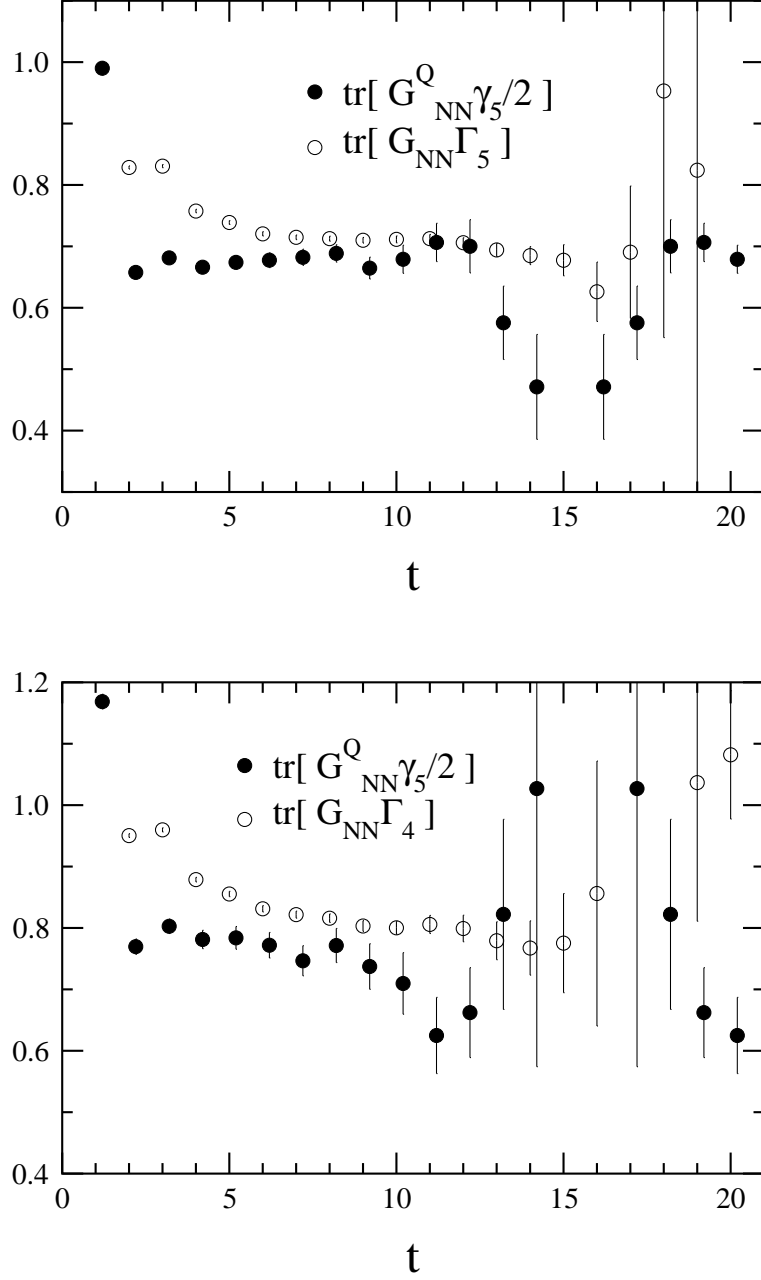


FIG. 11: Effective mass plot for the parity odd part of the nucleon propagator with Q (filled) for eq.eq.(56) $|\vec{p}| = 0$ (top) and eq.(57) $|\vec{p}| = 1$ (bottom) after averaged with backward propagator in time direction. The parity even part without Q (open), which are already shown in Fig. 8, are also plotted for comparison.

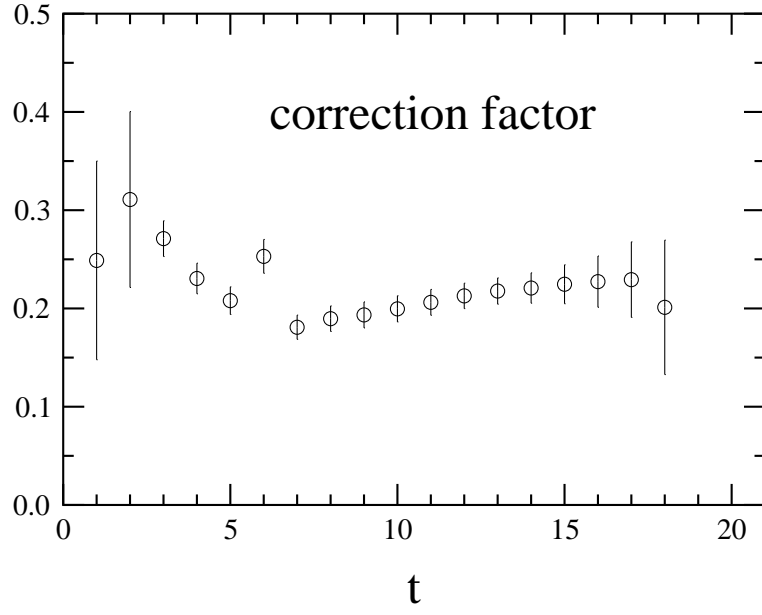


FIG. 12: Correction factor $R(q; \tau, t)$ as a function of t with $\tau = 6$ and $|\vec{q}| = 1$.

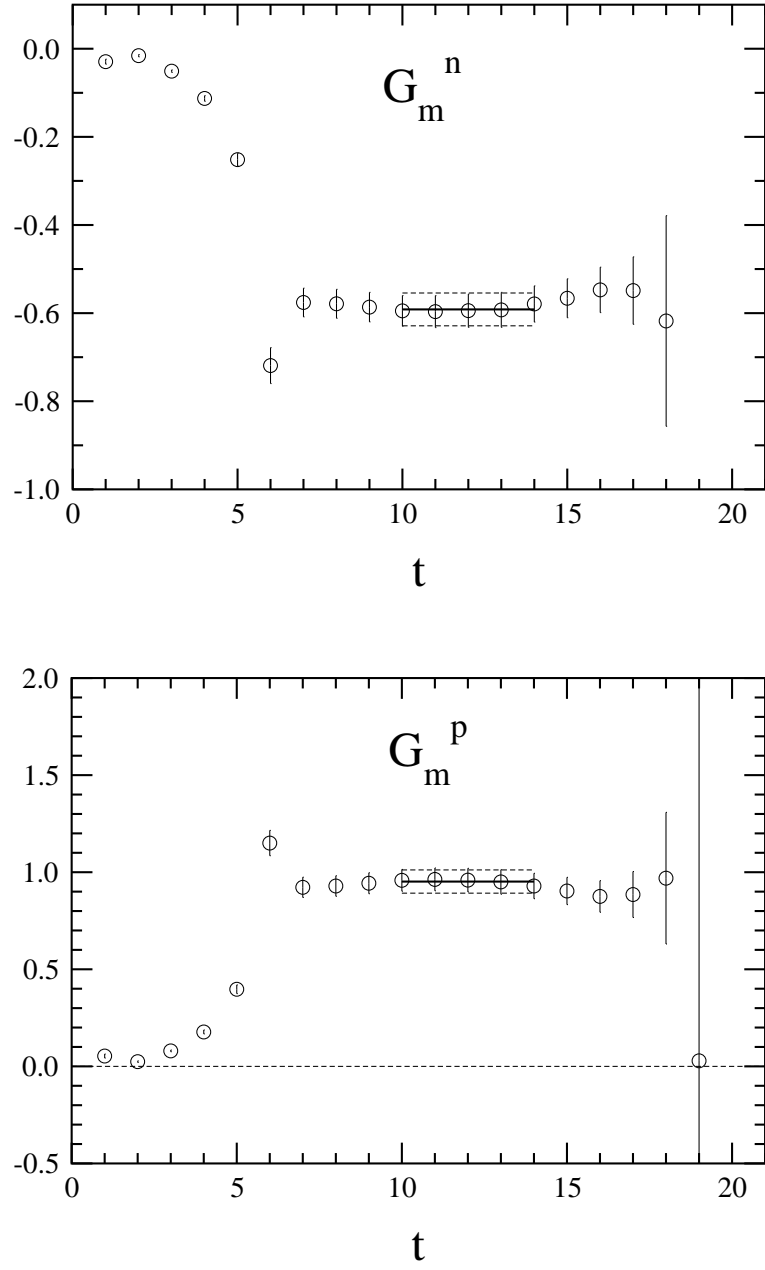


FIG. 13: Magnetic form factor for neutron (top) and proton (bottom).

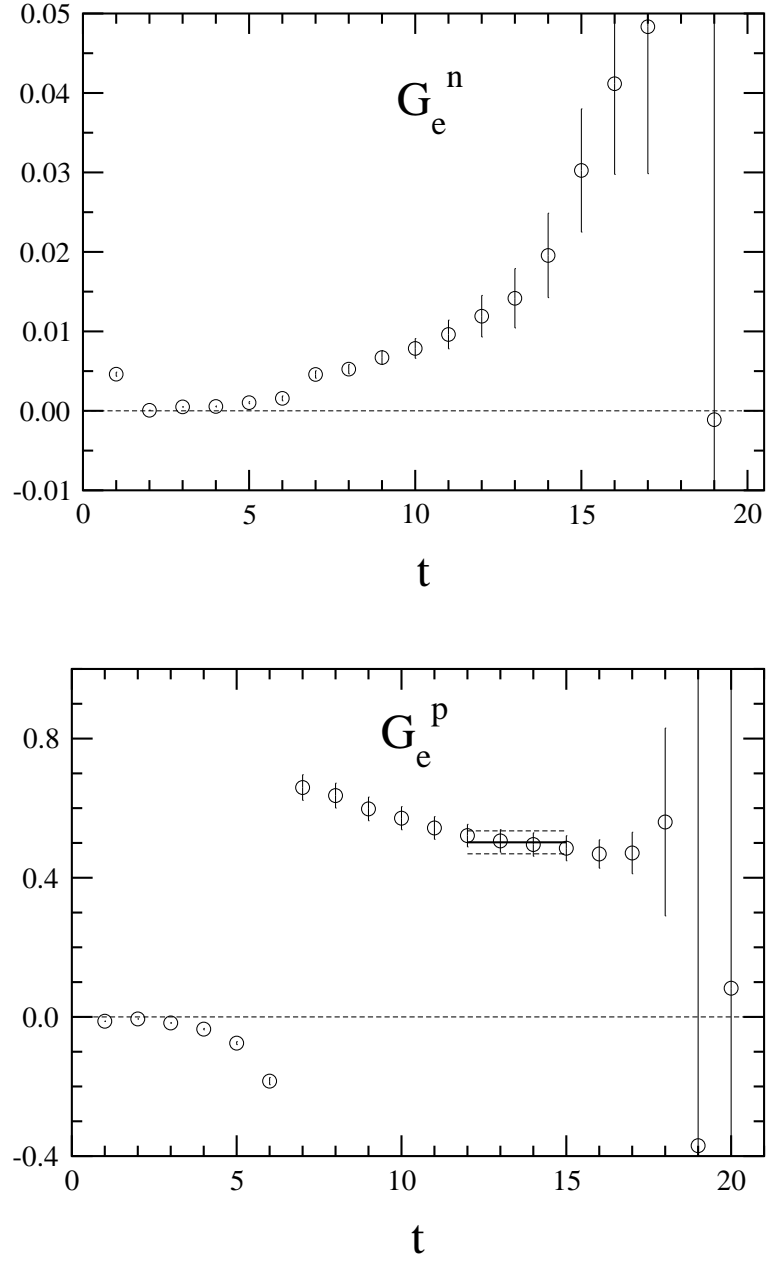


FIG. 14: Electric form factor for neutron (top) and proton (bottom).

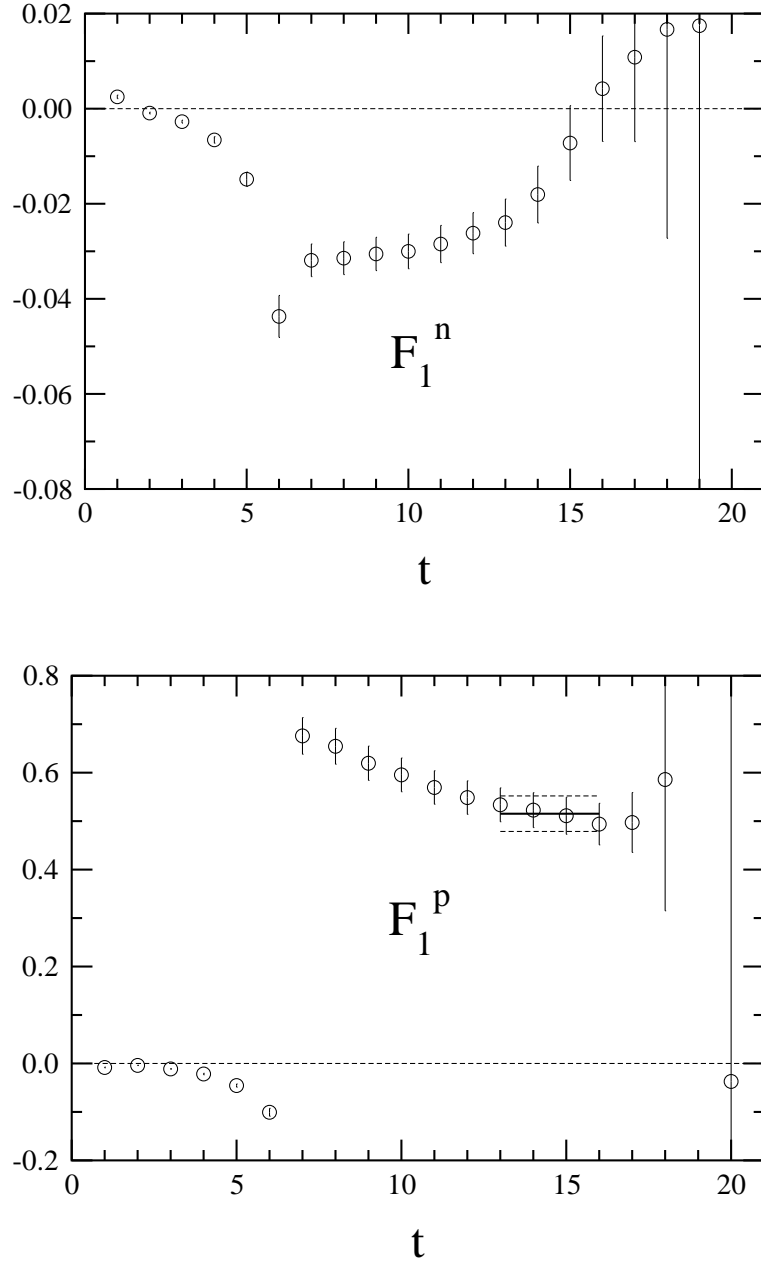


FIG. 15: Form factor $F_1(q^2)$ for neutron (top) and proton (bottom). Horizontal lines represent the constant fit.

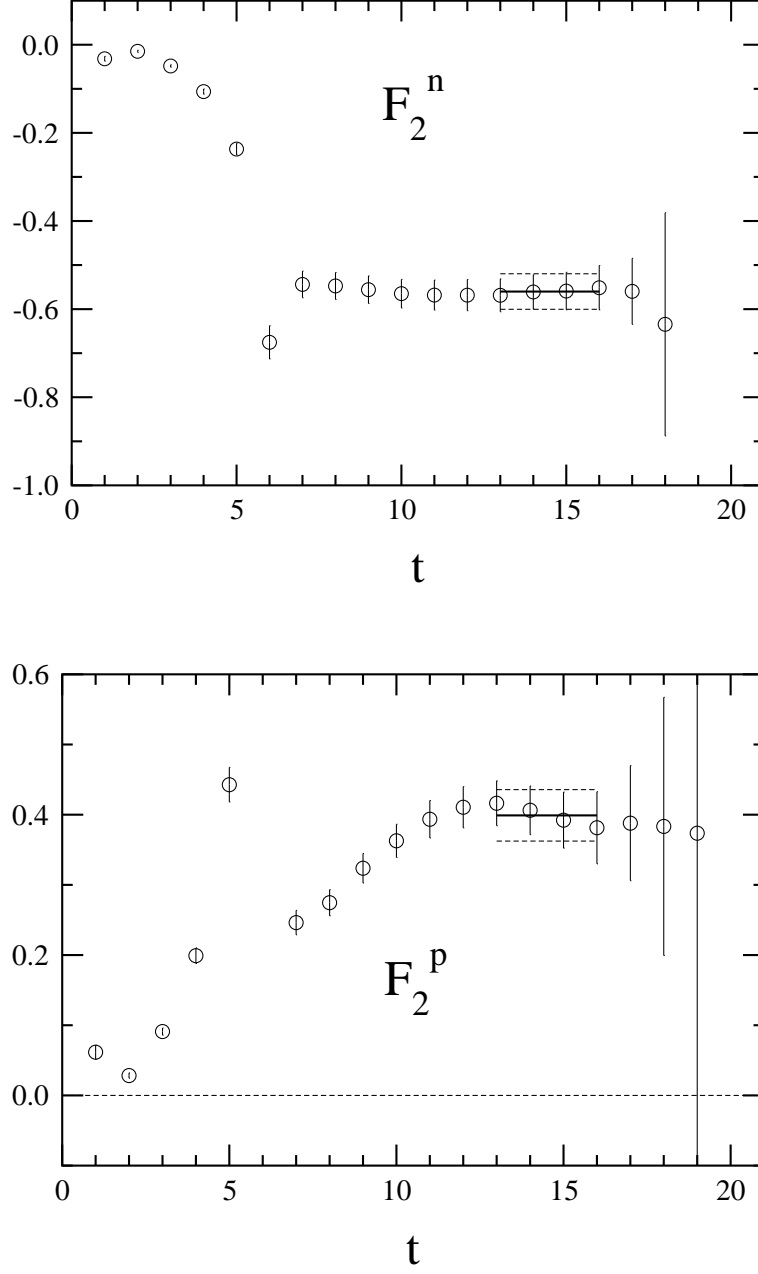


FIG. 16: Form factor $F_2(q^2)$ for neutron (top) and proton (bottom). Horizontal lines represent the constant fit.

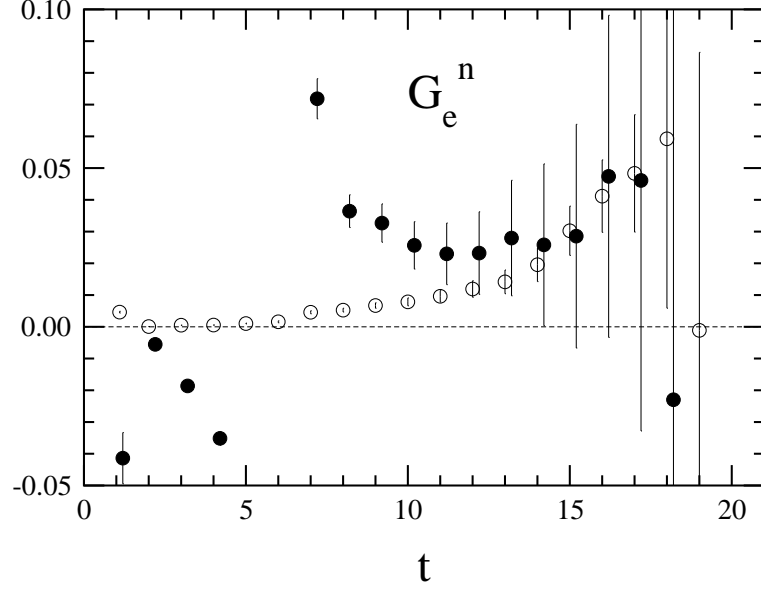


FIG. 17: Solid circles represent the electric form factor $G_e^n(q^2)$ for neutron in different analysis where the effect of N_- is taken into account, together with the previous result(open) in Fig.14.

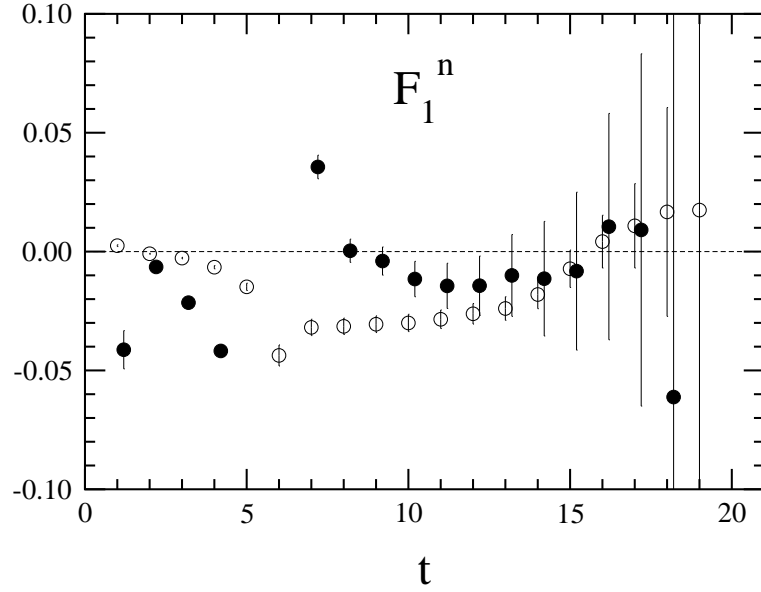


FIG. 18: Solid circles represent the form factor $F_1^n(q^2)$ for neutron in different analysis where the effect of N_- is taken into account, together with the previous result(open) in Fig.15.

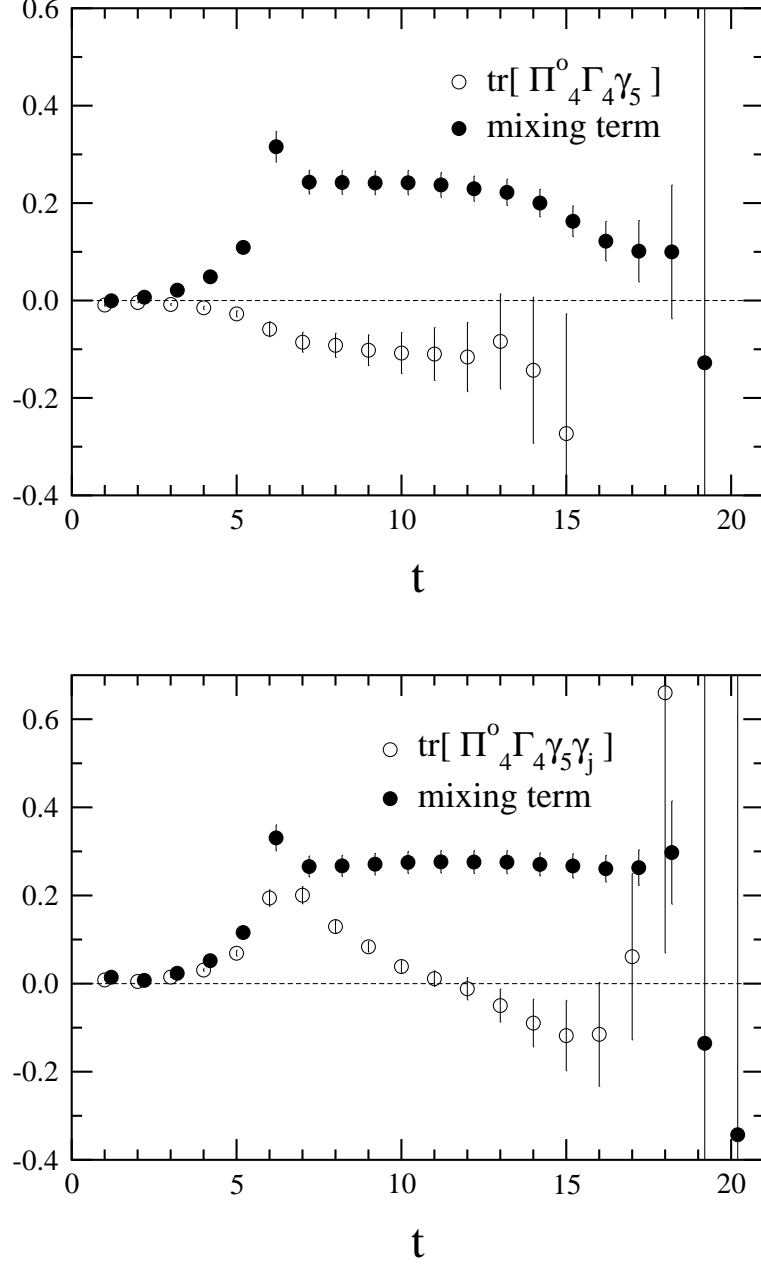


FIG. 19: Parity-odd part of the form factors for the neutron. Top: $\text{tr}[\Pi_4^o(q, t, \tau) \Gamma_4 \gamma_5]$ (open) and the mixing term (filled) in eq.(66). Bottom: $\text{tr}[\Pi_4^o(q, t, \tau) \Gamma_4 \gamma_5 \gamma_i]$ (open) and the mixing term (filled) in eq.(67).

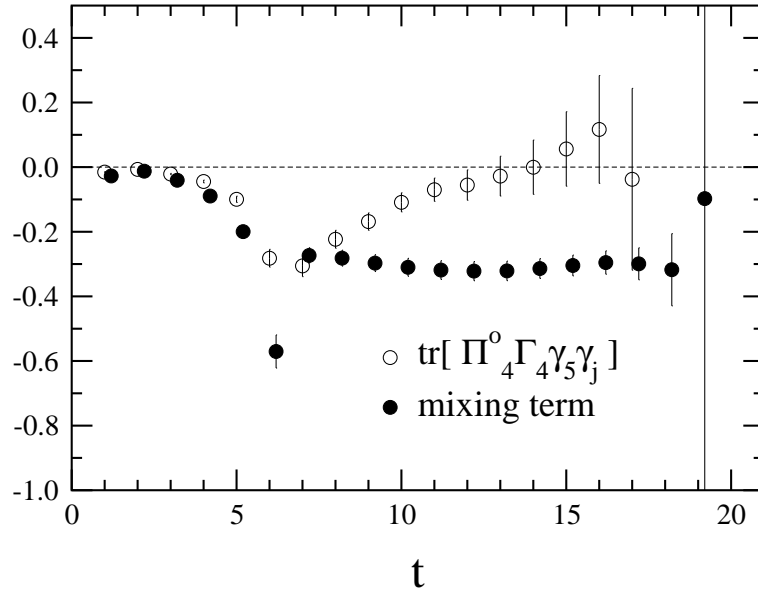
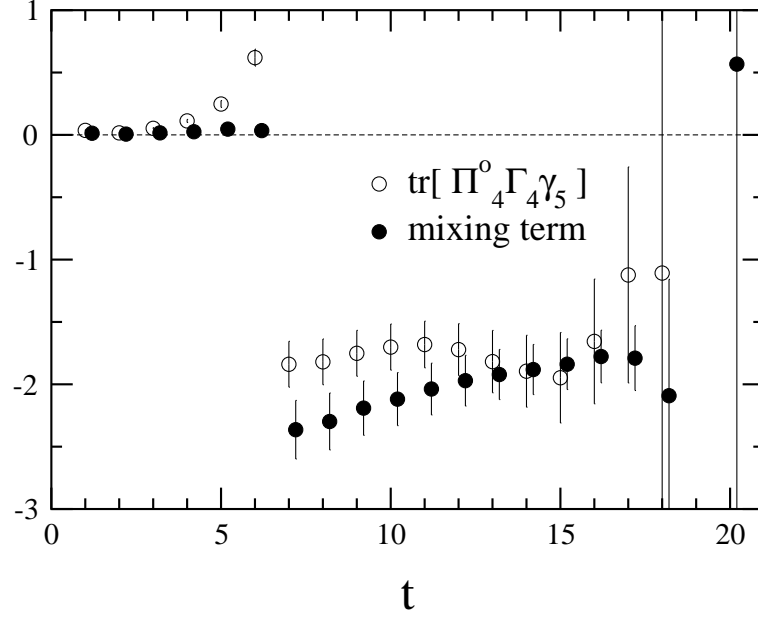


FIG. 20: Same quantities for the proton, as in the previous figure.

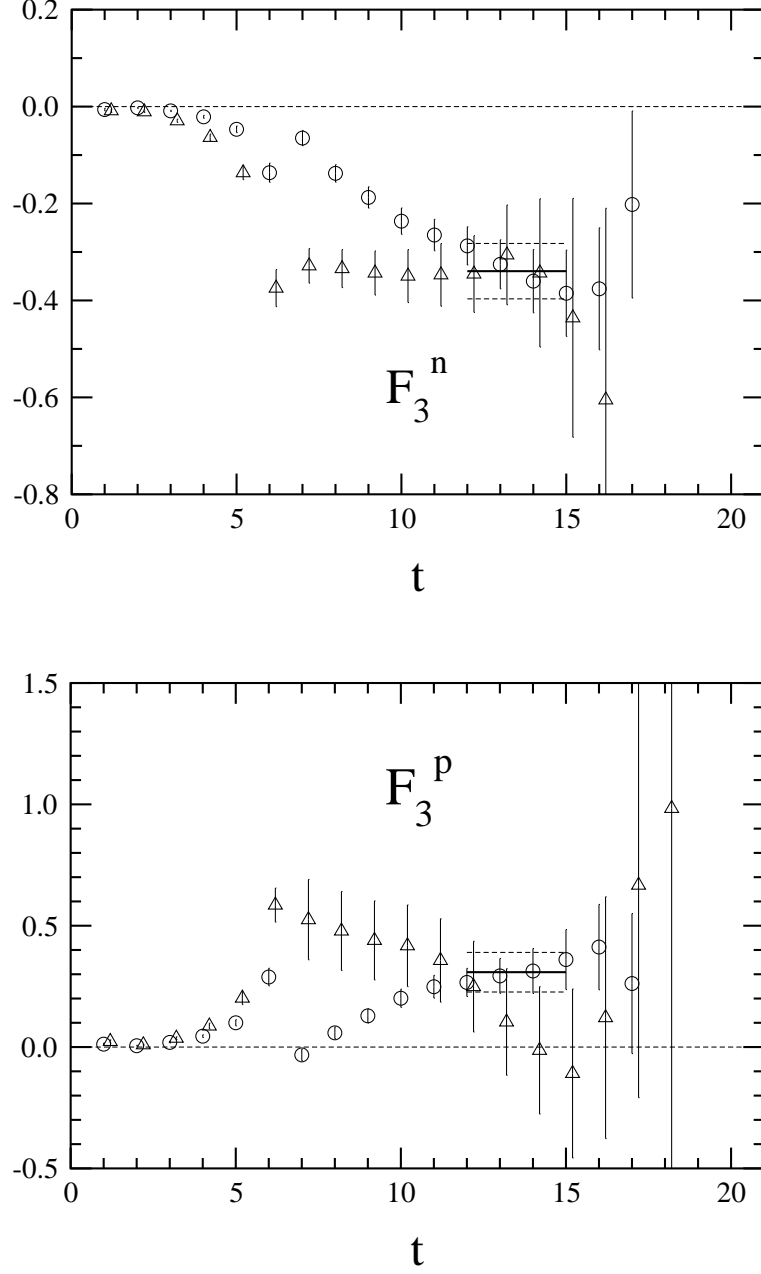


FIG. 21: The parity odd form factor F_3 for neutron (top) and proton (bottom). Circles represent the result with $\Gamma_4 \gamma_5$ projection of eq.(66), while triangles represent the one with $\Gamma_4 \gamma_5 \gamma_j$ projection averaged over $j = 1, 2, 3$ in eq.(67).

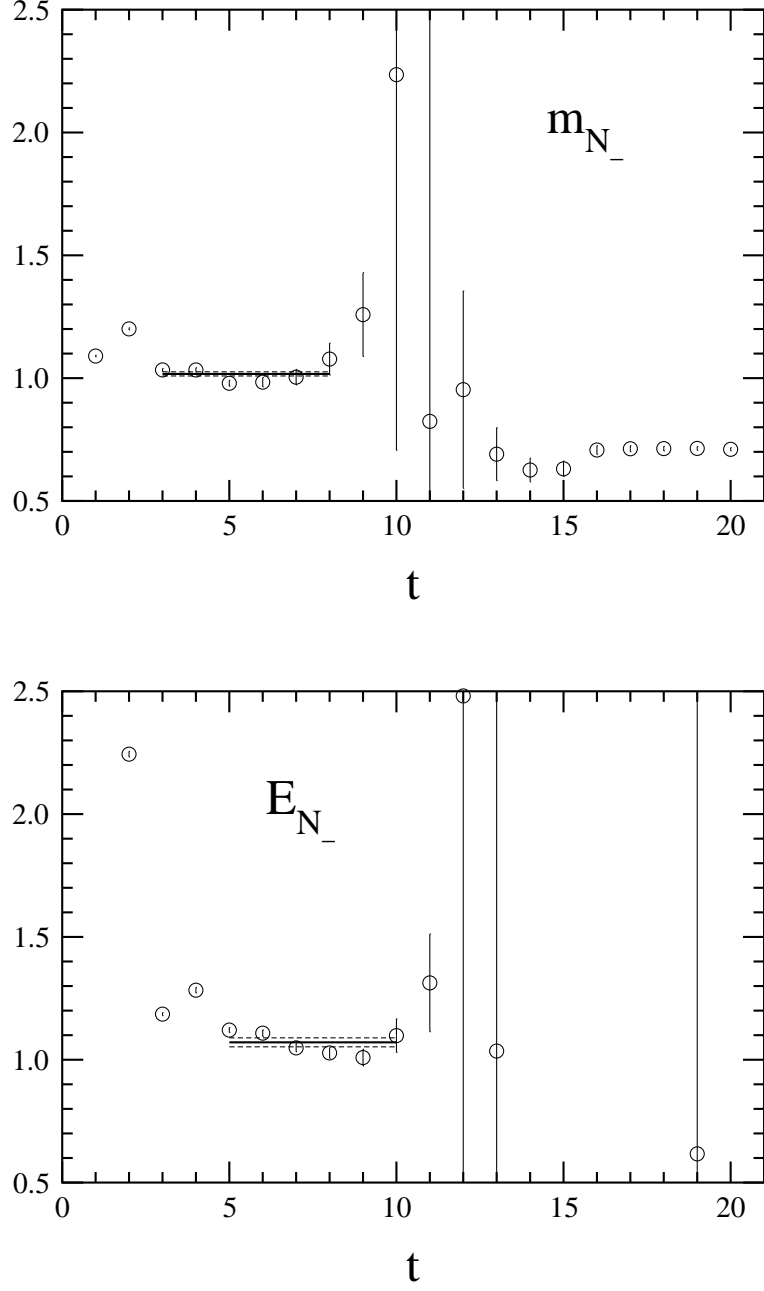


FIG. 22: Effective mass plot for the parity-odd nucleon for $|\vec{p}| = 0$ (top) and $|\vec{p}| = 1$ (bottom). Horizontal lines denote the central value (solid) and the errors (dotted) of the global fit.